Spring 5-5-2016

Boron Difluoride Formazanate Copolymers with 9,9-Di-n-hexylfluorene Prepared by Copper-Catalyzed Alkyne-Azide Cycloaddition Chemistry

Stephanie M. Barbon

Joe Gilroy
jgilroy5@uwo.ca

Boron Difluoride Formazanate Copolymers with 9,9-Di-*n*-hexylfluorene Prepared by Copper-Catalyzed Alkyne-Azide Cycloaddition Chemistry

*Stephanie M. Barbon and Joe B. Gilroy**

Department of Chemistry and the Centre for Advanced Materials and Biomaterials Research (CAMBR), The University of Western Ontario, 1151 Richmond St. N., London, Ontario, Canada, N6A 5B7. Tel: +1-519-661-2111 ext. 81561; E-mail: joe.gilroy@uwo.ca

TOC Graphic:

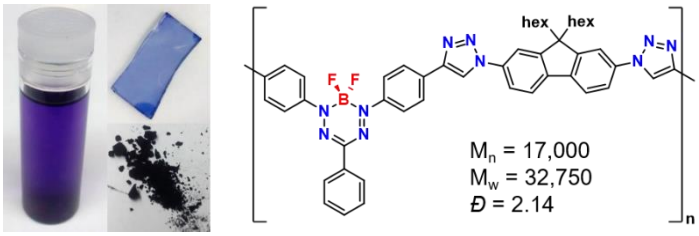

Abstract

The synthesis and characterization of copolymers based on boron difluoride formazanate (**BF_2L**) and 9,9-di-*n*-hexylfluorene (**hex_2Fl**) units are described. A series of model compounds [**(BF_2L)-(hex_2Fl)**, **(hex_2Fl)-(BF_2L)-(hex_2Fl)**, and **(BF_2L)-(hex_2Fl)-(BF_2L)**] were also studied in order to fully understand the spectroscopic properties of the title copolymer **[(BF_2L)-(hex_2Fl)]$_n$**. The model compounds and copolymers, which were synthesized by copper catalyzed alkyne-azide cycloaddition chemistry, exhibited high molar absorptivities (25,700–54,900 M^{-1} cm^{-1}), large Stokes shifts (123–143 nm, 3590–3880 cm^{-1}), and tunable electrochemical behaviour ($E°_{red1}$ *ca.* −0.75 V and $E°_{red2}$ *ca.* −1.86 V *vs.* ferrocene/ferrocenium). The low-energy wavelength of maximum absorption and emission of the model compounds red-shifted relative to the **BF_2L** repeating unit by *ca.* 30 nm per triazole ring formed, to maximum values of 557 nm and 700 nm in DMF, respectively. The low-energy absorption and emission properties of the copolymer were consistent with the model compound bearing two triazole rings [**(hex_2Fl)-(BF_2L)-(hex_2Fl)**] and were not dependant on copolymer molecular weight. However, the title copolymers may show promise as a light-harvesting material based on their thin-film optical band gap of 1.67 eV.

Introduction

Boron-containing polymers are of significant interest for a wide range of applications due to the unique properties resulting from the electron deficient nature of boron.[1-17] Polymers based on three- and four-coordinate boron centres have found application, for example, as sensors,[18-19] luminescent materials for biomedical imaging,[20] active materials in light emitting diodes,[21-22] electrolytes,[23] semi-conducting materials[10] and in photovoltaic devices.[24] The polymers used in these studies include boron in main-chain (*e.g.*, **1**, **2**) and side chain (*e.g.*, **3**, **4**) architectures.[25-28]

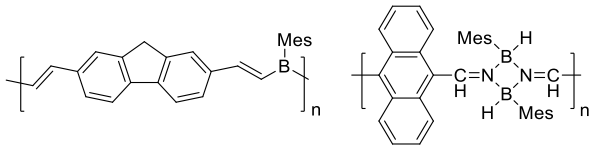

1 2

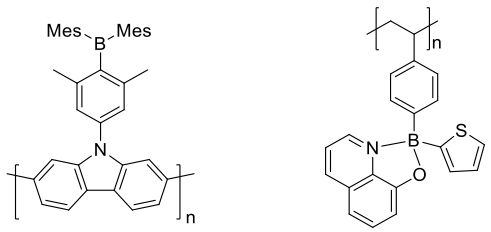

3 4

Of particular interest are polymers containing boron difluoride complexes of chelating ligands. The most common examples are based on BODIPY, aza-BODIPY or boron diketonate, ketiminate and diketiminate moieties.[3, 13] The resulting polymers often have high emission quantum yields, leading to their use in, for example, cell imaging (*e.g.*, **5**),[29-31] nanostructured dual emissive materials,[32] and as semiconductor materials for organic electronics (*e.g.*, **6**, **7**).[9-10]

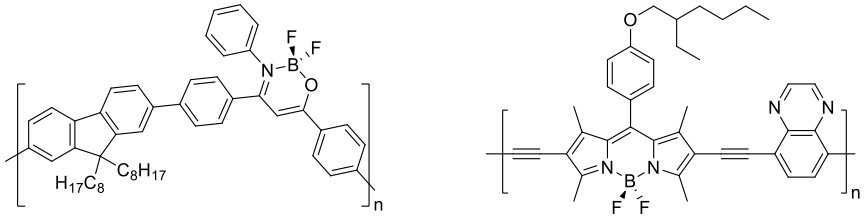

5 6

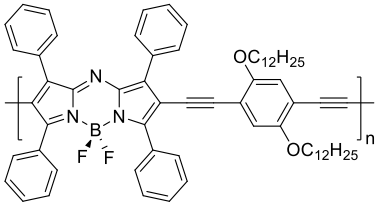

7

One class of boron complexes which has yet to be incorporated into π-conjugated polymers are boron difluoride complexes of formazanate ligands.[33] Metal and boron complexes of formazanate ligands have tunable optical and electronic properties.[34-45] In particular, boron

difluoride complexes have shown application as fluorescence cell-imaging agents,[46] as precursors to B(1)-carbenoid intermediates,[47] and as efficient electroluminescence emitters.[48] We have previously demonstrated that extending the π conjugation of BF_2 formazanates (*e.g.*, by replacing phenyl with naphthyl substituents), results in red-shifted wavelengths of maximum absorption and emission and increased emission quantum yields.[49] Considering these results, the incorporation of BF_2 formazanate complexes into π-conjugated copolymers is especially intriguing.

Herein, we describe the synthesis and characterization of the first examples of π-conjugated copolymers containing BF_2 formazanate complexes, synthesized by alkyne-azide cycloaddition chemistry. This 'click' reaction was chosen for its high efficiency, regioselectivity and functional group tolerance.[50-51] Since some of the first examples of 'click polymers' were reported in 2004,[52-53] alkyne-azide cycloaddition has been used to prepare polymers with application in nucleic acid delivery,[54] fluorescent photopatterning,[55] and photovoltaic applications.[56] We also present a comprehensive study of a series of model compounds designed to allow for the spectroscopic characteristics of the target copolymers to be fully understood.

Results and Discussion

Synthesis & Characterization

The copolymers and related model compounds described in this study were synthesized through copper-catalyzed [$Cu(PPh_3)_3Br$] alkyne-azide cycloaddition chemistry in THF, incorporating BF_2 complexes (**BF_2L**, **LH** = 1,3,5-triphenylformazan) and 9,9-di-*n*-hexylfluorene (**hex$_2$Fl**). Optimized reactions were carried out under nitrogen atmosphere for 18 h (48 h for copolymers) at 80 ^oC. The model compounds **hex$_2$Fl**, **BF_2L**, **(BF_2L)-(hex$_2$Fl), (hex$_2$Fl)-(BF_2L)-(hex$_2$Fl)**, and

(BF$_2$L)-(hex$_2$Fl)-(BF$_2$L) were fully characterized by ^{1}H, ^{11}B, ^{13}C{^{1}H and ^{19}F NMR spectroscopy, UV-vis absorption/emission and FT-IR spectroscopy and mass spectrometry (Figs. S1–S16). Copolymer **[(BF$_2$L)-(hex$_2$Fl)]$_n$** was subjected to similar analyses.

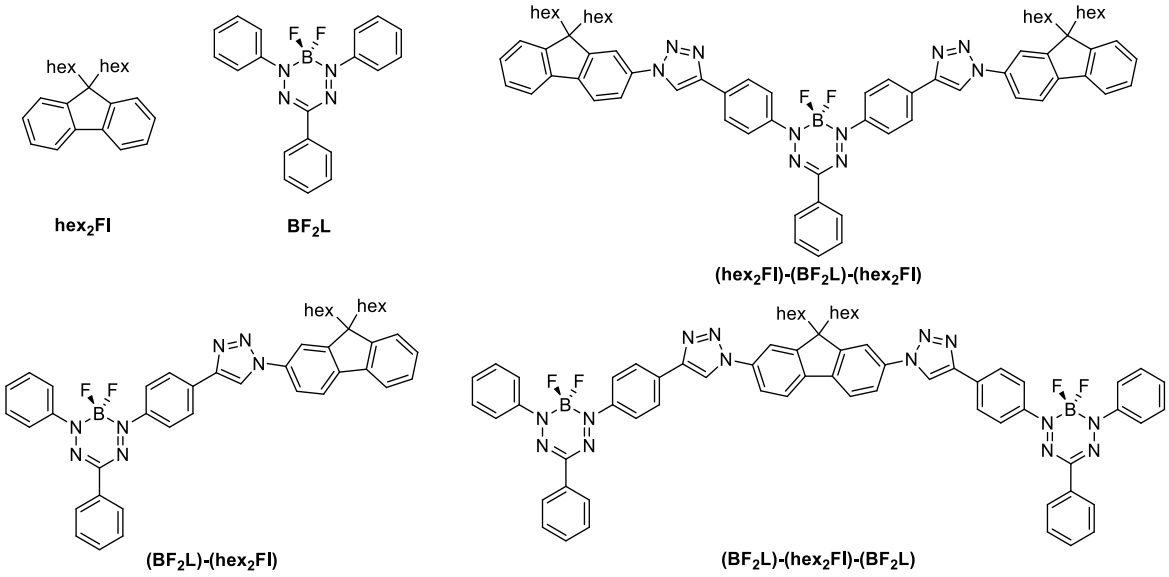

Polymerization reactions (Scheme 1) were monitored for 7 days by removing an aliquot of the reaction mixture after 12, 24, 48, 72 and 168 hours, and it was determined by GPC that the molecular weight reached a maximum after just 2 days (Figs. 1, S17). Decreasing the catalyst loading from 5% to 2% resulted in a decreased number average molecular weight (M_n) from 17,000 g mol^{-1} [Dispersity ($Đ$ = 2.14)] to 6,000 g mol^{-1} ($Đ$ = 2.13). Conditions were optimized to maximize molecular weight, while minimizing reaction times, and thus a catalyst loading of 5% and reaction time of 48 h was selected as the conditions to be used for all further polymerizations.

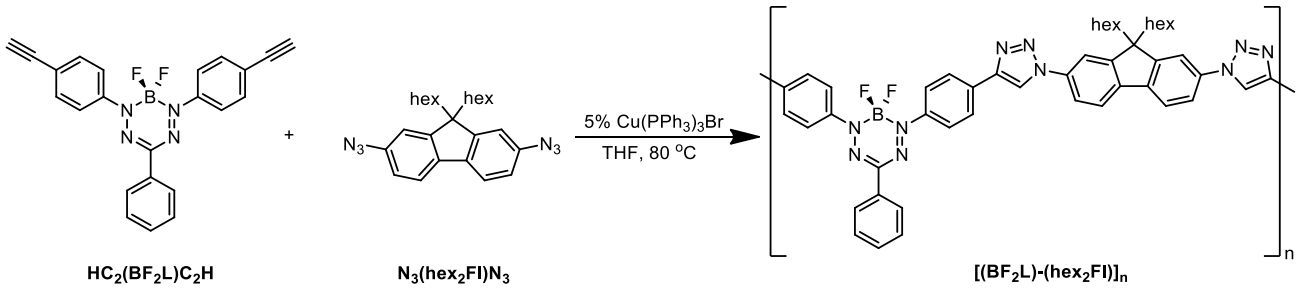

Scheme 1 Synthesis of copolymer **[(BF$_2$L)-(hex$_2$Fl)]$_n$** by copper-catalyzed alkyne-azide cycloaddition chemistry.

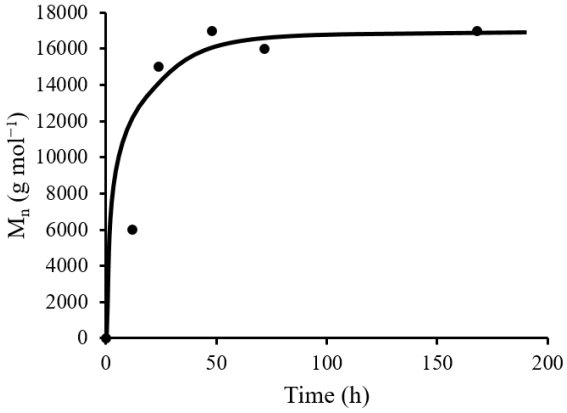

Fig. 1 Number average molecular weight of **[(BF$_2$L)-(hex$_2$Fl)]$_n$** as a function of reaction time. The black line has been added as a guide.

In the case of the copolymer, the successful incorporation of both the **BF$_2$L** and **hex$_2$Fl** repeating units was confirmed using NMR spectroscopy. We noted the disappearance of the terminal alkyne proton resonance (3.25 ppm), as well as the appearance of a singlet at 8.38 ppm, consistent with the presence of the triazole ring (Figs. 2, S18). The boron and fluorine signals in the ^{11}B and ^{19}F NMR spectra were retained (^{11}B NMR $\delta = -0.5$ ppm, ^{19}F NMR $\delta = -143.4$ ppm), indicating that the structure of the BF_2 formazanate complex had been maintained throughout the polymerization process. The molecular weight distribution of a representative sample of **[(BF$_2$L)-(hex$_2$Fl)]$_n$** after 2 days was determined by gel permeation chromatography (GPC), yielding a copolymer with M_n = 17,000 g mol^{-1} and $Đ$ = 2.14.

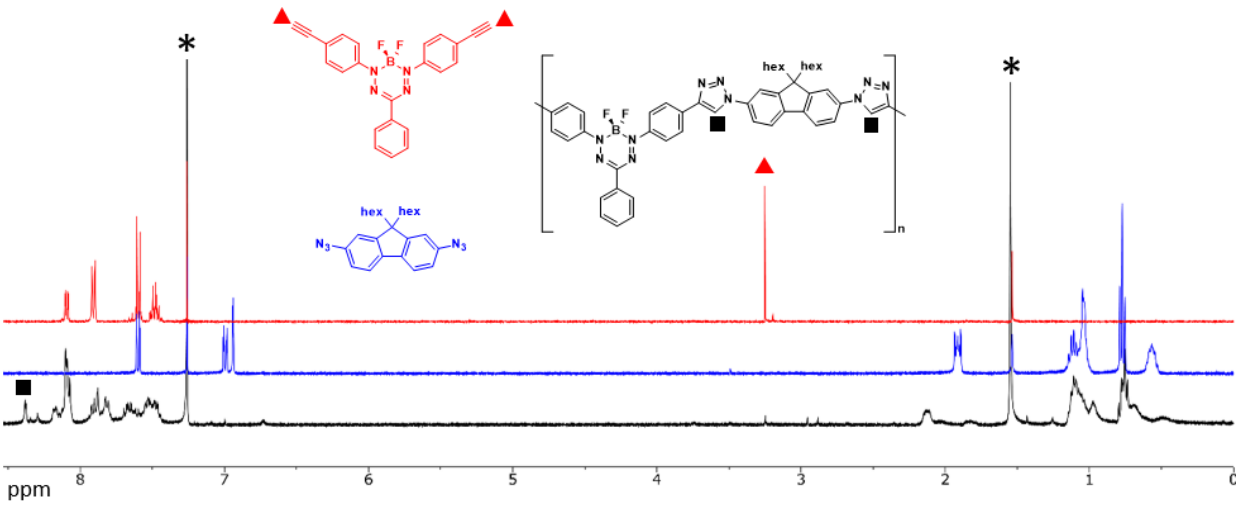

Fig. 2 ^{1}H NMR spectra of **HC$_2$(BF$_2$L)C$_2$H** (red), **N$_3$(hex$_2$Fl)N$_3$** (blue) and copolymer **[(BF$_2$L)-(hex$_2$Fl)]$_n$** (black) in $CDCl_3$. The asterisks denote residual solvent signals. The red triangle denotes the alkyne C-H signal in **HC$_2$(BF$_2$L)C$_2$H**, and the black square denotes the C-H signal formed by triazole formation in **[(BF$_2$L)-(hex$_2$Fl)]$_n$**.

Thermal gravimetric analysis (TGA) showed that **[(BF$_2$L)-(hex$_2$Fl)]$_n$** degraded gradually up to a temperature of 255 °C, at which time it had lost 3% of its mass. Above 255 °C, the copolymer degraded quickly to 55% of its original mass at 505 °C. Above 505 °C, slower degradation occured to a final 43% of the initial mass at 1,000 °C (Fig. S19). There was no observable glass transition (T_g) within the stability window (0 to 200 °C) determined for **[(BF$_2$L)-(hex$_2$Fl)]$_n$** (Fig. S20). Furthermore, there was also no observable melt transition in the differential scanning calorimetry (DSC) trace and both powder X-ray diffraction studies and scanning electron microscopy of a thin film of the copolymer confirmed its amorphous character (Figs. S21,S22).

Absorption and Emission Spectroscopy

The copolymer and each of the model compounds showed strong absorbance between 200−350 nm and 500−600 nm in DMF (Table 1). First, we consider the low-energy wavelength of

maximum absorption (λ_{max}), which has been previously attributed to a BF_2 formazanate π-π^* transition with HOMO→LUMO character (Fig. 3).[49] This transition in the copolymer (λ_{max} = 557 nm) is red-shifted by approximately 50 nm when compared to model compound **BF_2L** (λ_{max} = 505 nm). Furthermore, when we studied the same transition in model compound **(hex$_2$Fl)-(BF_2L)-(hex$_2$Fl)** (λ_{max} = 557 nm), it matched well with that of the copolymer. In both **[(BF_2L)-(hex$_2$Fl)]$_n$** and **(hex$_2$Fl)-(BF_2L)-(hex$_2$Fl)**, each BF_2L unit is bound to two triazole rings, potentially extending the degree of π conjugation. We also note that the same absorption in **(BF_2L)-(hex$_2$Fl)** (λ_{max} = 533 nm), which has just one triazole bound to the **BF_2L** moiety, was red-shifted by just 28 nm. Based on these results, we concluded that the introduction of each triazole ring shifted the formazanate λ_{max} by approximately 30 nm. The similarity between copolymer **[(hex$_2$Fl)-(BF_2L)]$_n$** and the model compounds also suggested that the properties of the copolymer are not dictated by long range π conjugation along the polymer backbone. However, the λ_{max} of **[(hex$_2$Fl)-(BF_2L)]$_n$** is significantly lower in energy compared to the π-conjugated boron ketoiminate polymer **5** (λ_{max} = 300 nm, THF),[31] and comparable to the π-conjugated BODIPY system (**6**, λ_{max} = 596 nm, $CHCl_3$).[10]

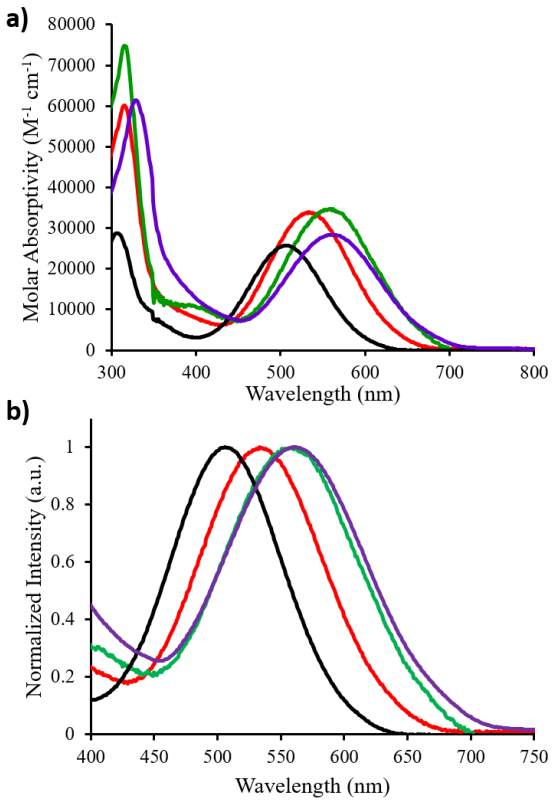

Fig. 3 a) UV-vis absorption spectra of **BF_2L** (black), **(BF_2L)-(hex$_2$Fl)** (red), **(hex$_2$Fl)-(BF_2L)-(hex$_2$Fl)** (green) and **[(BF_2L)-(hex$_2$Fl)]$_n$** (purple), recorded for 10^{-5} M DMF solutions. b) Normalized UV-vis absorption spectra from 400−750 nm for comparison.

Next, we considered the high-energy absorption maxima for these compounds (Fig. 4). This region is complex, as both **hex$_2$Fl** and **BF_2L** absorb between 200–350 nm. When considering the 9,9-di-*n*-hexylfluorene contributions, we observed a similar trend to that of the absorption of the BF_2 formazanate unit. The high-energy absorption band of copolymer **[(BF_2L)-(hex$_2$Fl)]$_n$** (λ_{max} = 327 nm) was red-shifted by 23 nm, when compared to **hex$_2$Fl** (λ_{max} = 304 nm). Again, we attributed the red-shift to extended π conjugation relating to the presence of the triazole rings bound to 9,9-di-*n*-hexylfluorene. Model compound **(BF_2L)-(hex$_2$Fl)** has a high energy wavelength of maximum absorption (λ_{max} = 317 nm) which falls almost exactly half way between the wavelength of maximum absorption of **hex$_2$Fl** and **[(BF_2L)-(hex$_2$Fl)]$_n$**, further

corroborating our conclusion that the observed trends in electronic properties arise due to the presence of the triazole rings and not extended π conjugation of the copolymer backbone. The observed trends are consistent with similar compounds synthesized by alkyne-azide cycloaddition chemistry.[55, 57-58] We also note that the absorption profile is unchanged with variation in the molecular weight of the **[(BF$_2$L)-(hex$_2$Fl)]$_n$** (Fig. S23). The thin-film absorption spectra of **[(BF$_2$L)-(hex$_2$Fl)]$_n$** and all model compounds were red-shifted with respect to the solution-based spectra by *ca.* 20 nm, but were qualitatively similar, indicating the formation of J-aggregates (Fig. S24). The estimated band gap (E_g) of 1.67 eV (Table 2), indicates that, despite the lack of long range π conjugation in **[(BF$_2$L)-(hex$_2$Fl)]$_n$**, it may find use as a light harvesting material in organic electronics.

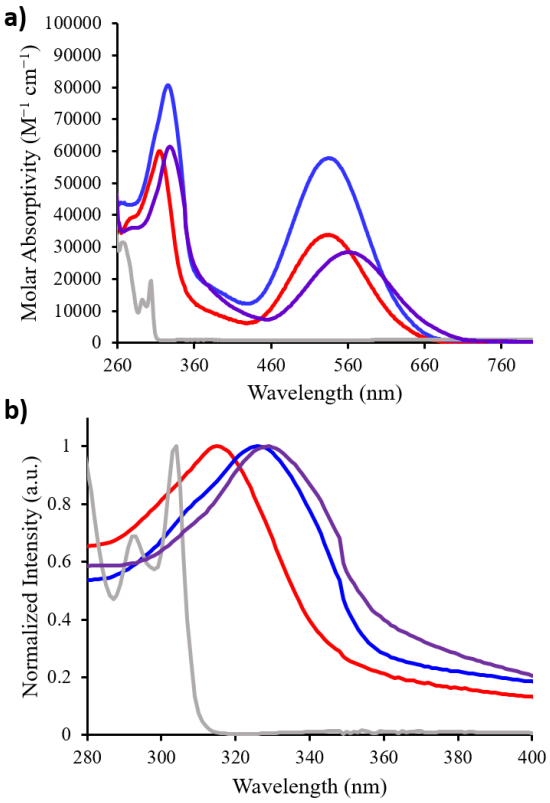

Fig. 4 a) UV-vis absorption spectra of **hex$_2$Fl** (grey), **(BF$_2$L)-(hex$_2$Fl)** (red), **(BF$_2$L)-(hex$_2$Fl)-(BF$_2$L)** (blue) and **[(BF$_2$L)-(hex$_2$Fl)]$_n$** (purple) recorded for 10^{-5} M DMF solutions. b) Normalized UV-vis absorption spectra for 280−400 nm region for comparison.

Each of the model compounds are weakly emissive in solution, with fluorescence quantum yields (Φ_F) of < 3% in DMF (Table 1) and Stokes shifts (ν_{ST}) ranging from 123−143 nm (3590−3880 cm^{-1}). The copolymer **[(BF$_2$L)-(hex$_2$Fl)]$_n$**, exhibits two emission maxima when excited at 327 nm. The first is a broad, bimodal signal, with a wavelength of maximum emission (λ_{em}) at 352 nm. The second maxima at 669 nm was consistent with the emission spectra of BF_2 formazanates (Fig. S25).[39] The fact that the intense emission normally associated with **hex$_2$Fl** has been quenched leads us to believe that a photoinduced electron transfer (PET) mechanism may be implicated for these systems. However, as the high energy absorption/emission bands for **BF$_2$L** and **hex$_2$Fl** overlap, we were unable to probe this behavior further. The emission spectra of the copolymers were also unchanged with variation in molecular weight (Fig. S23). The emission spectra for the model compounds were qualitatively similar to the copolymer, with the high energy emission maxima generally decreasing in intensity when the ratio of **BF$_2$L** to **hex$_2$Fl** units was increased (Table 1). All of the compounds reported in this study were non-emissive in the solid state.

Table 1. Summary of absorption/emission and electrochemical properties in DMF and as thin films.

	$\lambda_{max,\ DMF}$ (nm)	$\lambda_{max,\ film}$ (nm)	$\lambda_{em,\ DMF}$ (nm)	$\Phi_{F,\ DMF}$ (%)[a]	$\nu_{ST,\ DMF}$ (nm)	$\nu_{ST,\ DMF}$ (cm^{-1})	$E°_{red1}$[c] (V)	$E°_{red2}$[c] (V)
hex$_2$Fl	304	-	317	41.5	13	1350	-	-
BF$_2$L	306	-	338	0.2	32	3090	−0.80	−2.00
	505	525	628		123	3880		
(BF$_2$L)-(hex$_2$Fl)	317	-	352	2.3	35	3140	−0.77	−1.84
	533	554	669		136	3810		
(hex$_2$Fl)-(BF$_2$L)-(hex$_2$Fl)	314	-	382	2.2	68	5670	−0.75	−1.86
	557	583	700		143	3670		
(BF$_2$L)-(hex$_2$Fl)-(BF$_2$L)	326	-	383	2.0	57	4560	−0.78	−1.93
	533	559	670		137	3840		
[(BF$_2$L)-(hex$_2$Fl)]$_n$	327	-	382	1.2	55	4400	−0.73	−1.76[b]
	557	586	696		139	3590		

[a]Quantum yields were measured using ruthenium tris(bipyridine) hexafluorophosphate as a relative standard[59-60] and corrected for wavelength-dependent detector sensitivity (Fig. S26). [b]Onset of irreversible reduction, cathodic peak potential quoted. [c]Cyclic voltammetry experiments were conducted in DMF containing 1 mM analyte and 0.1 M *n*Bu_4PF_6 as supporting electrolyte at a scan rate of 250 mV s^{-1}. All voltammograms were referenced internally against the ferrocene/ferrocenium redox couple.

Cyclic Voltammetry

The electrochemical properties of copolymer **[(BF$_2$L)-(hex$_2$Fl)]$_n$** and each of the model compounds are dominated by the **BF$_2$L** fragments, as 9,9-di-*n*-hexylfluorene is not redox-active within the electrochemical window of DMF (Fig. S27). All model compounds gave rise to two reversible one-electron reduction waves per **BF$_2$L** unit in their cyclic voltammograms (Figs. S28–S31). The first reduction corresponds to the formation of a ligand-centered radical anions, and the second to ligand-centered dianions.[37-38, 61] The copolymer **[(BF$_2$L)-(hex$_2$Fl)]$_n$** had broadened electrochemical features, including a chemically-reversible one-electron reduction at $E°_{red1}$ = −0.73 V *vs*. the ferrocene/ferrocenium redox couple, and a second one-electron irreversible reduction at an onset potential, E_{pc} = −1.76 V (Fig. 5). We also consistently observed the presence of a small irreversible oxidation process over multiple experiments at an onset of

E_{pa} = 0.35 V. The first reduction potentials ($E°_{red1}$) of the compounds and copolymer follow a logical trend with the number of triazoles present in the compound (Table 2). The model compound with no triazoles present (**BF_2L**) is the most difficult to reduce, at $E°_{red1}$ = −0.80 V. Adding one triazole, in model compounds **(BF_2L)-(hex$_2$Fl)-(BF_2L)** and **(BF_2L)-(hex$_2$Fl)** makes the BF_2 formazanate slightly easier to reduce ($E°_{red1}$: −0.77 V and −0.78 V, respectively). Finally, compound **(hex$_2$Fl)-(BF_2L)-(hex$_2$Fl)** with two triazoles is the easiest model compound to reduce, with a first reduction potential of −0.75 V, very similar to that of **[(BF_2L)-(hex$_2$F)]$_n$** ($E°_{red1}$ = −0.73 V). The energies of the lowest occupied molecular orbital (E_{LUMO}) for each species were estimated from the onset of the first reduction, and ranged from −4.79 to −4.81 eV (Table 2).

Table 2. Optical and electrochemical band gaps and HOMO/LUMO energies.

	E_g (nm)[a]	**E_g (eV)**[a]	**E_{LUMO} (eV)**[b]	**E_{HOMO} (eV)**[c]
BF_2L	660	1.88	−4.74	−6.62
(BF_2L)-(hex$_2$Fl)	703	1.76	−4.75	−6.51
(hex$_2$Fl)-(BF_2L)-(hex$_2$Fl)	736	1.68	−4.77	−6.45
(BF_2L)-(hex$_2$Fl)-(BF_2L)	700	1.77	−4.76	−6.53
[(BF_2L)-(hex$_2$Fl)]$_n$	744	1.67	−4.81	−6.48

[a]Estimated from the onset of absorption in the thin-film UV-vis spectra. [b]Estimated from the onset of the first electrochemical reduction, with the ferrocene/ferrocenium oxidation set at a potential of 5.39 eV.[62] [c]Estimated from the E_{LUMO} level and the optical band gap.

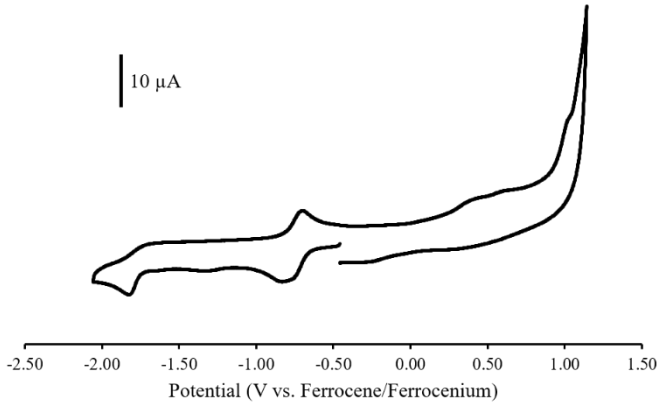

Fig. 5 Cyclic voltammogram of **[(BF$_2$L)-(hex$_2$Fl)]$_n$** recorded at 250 mV s^{-1} in a 1 mM DMF solution containing 0.1 M *n*Bu$_4$NPF$_6$ as supporting electrolyte.

Conclusions

In conclusion, we have successfully synthesized the first π-conjugated copolymers based on BF_2 formazanate complexes. Comparing the absorption spectra of model compounds with that of the copolymer indicate that π conjugation of the **BF$_2$L** and **hex$_2$Fl** units does not extend beyond the triazole groups formed by alkyne-azide cycloaddition. The addition of each triazole unit shifts the wavelengths of maximum absorption and emission of both units by *ca.* 30 nm, and also make the compounds easier to reduce by *ca.* 30 mV. Based on the thin-film UV-vis absorption spectra we estimate an optical band gap of 1.67 eV for the copolymer, highlighting the potential application of this material in organic light-harvesting devices. Our future work in this area will focus on the direct coupling of BF_2 formazanate fragments to π-conjugated organic spacers in order to further increase the extent of π conjugation along the backbone of BF_2 formazanate polymers.

Experimental Section

General Considerations

All reactions and manipulations were carried out under a nitrogen atmosphere using standard Schlenk techniques unless otherwise stated. Solvents were obtained from Caledon Laboratories, dried using an Innovative Technologies Inc. solvent purification system, collected under vacuum and stored under a nitrogen atmosphere over 4 Å molecular sieves. All reagents were purchased from Sigma-Aldrich or Alfa Aesar and used as received. **N_3(hex$_2$Fl)N_3**,[63] **hex$_2$Fl**,[64] **LH**[65] and **BF_2L**[49] were prepared according to literature procedures.

NMR spectra were recorded on 400 MHz (^{1}H: 399.8 MHz, ^{11}B: 128.3 MHz, ^{19}F: 376.1 MHz) or 600 MHz (^{1}H: 599.5 MHz, ^{13}C: 150.8 MHz) Varian INOVA instruments. ^{1}H NMR spectra were referenced to residual $CHCl_3$ (7.26 ppm) and ^{13}C NMR spectra were referenced to $CDCl_3$ (77.2 ppm). ^{11}B spectra were referenced to $BF_3{\cdot}OEt_2$ at 0 ppm and ^{19}F spectra were referenced to $CFCl_3$ at 0 ppm. Mass spectrometry data were recorded in positive-ion mode on a high-resolution Finnigan MAT 8200 spectrometer using electron impact ionization or a Micromass LCT electrospray time-of-flight mass spectrometer. UV-vis absorption spectra were recorded using Cary 300 or Cary 5000 instruments. Four separate concentrations were run for each sample and molar extinction coefficients were determined from the slope of a plot of absorbance against concentration. Thin-film absorption spectra were recorded for films prepared by spin coating onto glass from a 15 mg mL^{-1} solution in chlorobenzene at room temperature. Infrared spectra were recorded on a KBr disk using a Bruker Vector 33 FT-IR spectrometer. Emission spectra were obtained using a Photon Technology International QM-4 SE spectrofluorometer. Excitation wavelengths were chosen based on λ_{max} from the respective UV-vis absorption spectrum in the same solvent. Emission quantum yields were estimated relative to

ruthenium tris(bipyridine) hexafluorophosphate and corrected for wavelength dependent detector sensitivity (Fig. S24).[60] Powder samples of **[(BF$_2$L)-(hex$_2$Fl)]$_n$** were analyzed using an Inel CPS powder diffractometer with a CuKα source of λ = 1.5406 Å.

Electrochemical Methods

Cyclic voltammetry experiments were performed with a Bioanalytical Systems Inc. (BASi) Epsilon potentiostat and analyzed using BASi Epsilon software. Electrochemical cells consisted of a three-electrode setup including a glassy carbon working electrode, platinum wire counter electrode and silver wire *pseudo* reference electrode. Experiments were run at scan rates of 100 or 250 mV s^{-1} in degassed DMF solutions of the analyte (~1 mM) and supporting electrolyte (0.1 M *n*Bu_4PF_6). Cyclic voltammograms were referenced against an internal standard (~1 mM ferrocene) and corrected for internal cell resistance using the BASi Epsilon software.

Gel permeation chromatography (GPC)

GPC experiments were conducted in chromatography grade DMF at concentrations of 5 mg mL^{-1} using a Waters 2695 separations module equipped with a Waters 2414 differential refractometer and two PLgel 5 m mixed-D (300 × 7.5 mm) columns from Polymer Laboratories connected in series. The calibration was performed using polystyrene standards.

Thermal Analysis

Thermal degradation studies were performed using a TA Instruments Q50 TGA. A sample of copolymer **[(BF$_2$)-(hex$_2$Fl)]$_n$** was placed in a platinum pan and heated at a rate of 10 °C min^{-1} from room temperature to 1,000 °C under a flow of nitrogen (100 mL min^{-1}). Differential Scanning Calorimetry studies were performed on a TA Instruments DSC Q2000. A sample of copolymer **[(BF$_2$)-(hex$_2$Fl)]$_n$** was placed in an aluminum Tzero pan and heated from 20 °C to

200 °C at 10 °C min^{-1} under a flow of nitrogen (50 mL min^{-1}) and cooled down to 20 °C at 10 °C min^{-1}, before the sample underwent two additional heating/cooling cycles.

Scanning Electron Microscopy

Thin films of copolymer **[(BF$_2$L)-(hex$_2$Fl)]$_n$** were prepared by spin coating (150 rpm, 10 s, then 2000 rpm, 30 s) a 15 mg mL^{-1} solution of **[(BF$_2$L)-(hex$_2$Fl)]$_n$** in chlorobenzene at room temperature onto silicon wafers. The surface morphology was assessed directly by scanning electron microscopy (SEM) at 2 keV beam energy using the LEO/Zeisss 1530 instrument at the Western Nanofabrication Facility.

Preparation of (hex$_2$Fl)N$_3$

2-Bromo-9,9-di-*n*-hexylfluorene (2.50 g, 6.05 mmol) was dissolved in dry THF (125 mL) and cooled to −78 °C. *n*-BuLi (5.5 mL of a 2.5 M solution in hexanes, 14 mmol) was added slowly via a dropping funnel over a 20 min period. Upon addition, the solution turned a bright yellow color, and was stirred for 90 min at −78 °C. Tosyl azide (2.72 g, 13.8 mmol) was dissolved in 25 mL dry THF and added slowly to the 9,9-di-*n*-hexylfluorene solution, causing it to change to a dark orange/brown color. The reaction was warmed to room temperature and stirred for an additional 18 h. Deionized H_2O (10 mL) was then added to quench any excess *n*-BuLi, and the organics were extracted into CH_2Cl_2, dried over $MgSO_4$, gravity filtered and concentrated *in vacuo*. The resulting residue was purified by flash chromatography (petroleum ether, silica) to yield a light yellow oil. Yield = 0.58 g, 26%. ^{1}H NMR (599.5 MHz, $CDCl_3$) δ 7.67−7.64 (m, 2H, aryl C*H*), 7.33−7.27 (m, 3H, aryl C*H*), 7.01−6.98 (m, 2H, aryl C*H*), 1.99−1.89 (m, 4H, alkyl C*H*), 1.14−1.03 (m, 12H, alkyl C*H*), 0.77 (t, $^3J_{HH}$ = 7 Hz, 6H, alkyl C*H*), 0.62−0.57 (m, 4H, alkyl C*H*). ^{13}C{^{1}H} NMR (100.6 MHz, $CDCl_3$): δ 153.1, 150.6, 140.5, 138.9, 138.6, 127.2, 127.1, 123.0, 120.9, 119.6, 117.9, 113.8, 55.4, 40.6, 31.7, 29.9, 23.9, 22.8, 14.2. FT-IR (KBr):

2938 (m), 2926 (s), 2856 (m), 2102 (s), 1559 (m), 1456 (m), 1375 (w), 1291 (m), 1123 (w), 1084 (w), 817 (m), 736 (m) cm^{-1}. UV-vis (CH_2Cl_2): λ_{max} = 276 nm (ε = 23,800 M^{-1} cm^{-1}). Mass Spec. (EI, +ve mode): exact mass calculated for $[C_{25}H_{33}N_3]^+$: 375.2674; exact mass found: 375.2669; difference: −1.3 ppm.

Preparation of HC_2(LH)

In air, phenylhydrazine (0.9 g, 0.8 mL, 9 mmol) was dissolved in ethanol (10 mL) before benzaldehyde (0.9 g, 0.9 mL, 9 mmol) was added and the solution stirred for 10 min. After this time, a light yellow precipitate had formed and CH_2Cl_2 (75 mL) and deionized H_2O (75 mL) were added to form a biphasic reaction mixture. Na_2CO_3 (2.88 g, 27.2 mmol) and *n*Bu_4NBr (0.27 g, 0.85 mmol) were added, and the mixture was cooled with stirring for 30 min in an ice bath to 0 °C. In a separate flask, 4-ethynylaniline (1.00 g, 8.50 mmol) and concentrated HCl (2.2 mL, 26 mmol) were mixed in deionized H_2O (15 mL) and cooled in an ice bath. A cooled solution of sodium nitrite (0.67 g, 9.7 mmol) in deionized H_2O (5 mL) was added slowly to the amine solution over a 5 min period. This mixture was then stirred at 0 °C for 30 min, after which time it was added dropwise to the biphasic reaction mixture described above over a 10 min period. The resulting solution was stirred for 18 h, gradually turning dark red over this time. The dark red organic fraction was then washed with deionized H_2O (3 × 50 mL), dried over $MgSO_4$, gravity filtered and concentrated *in vacuo*. The resulting residue was purified by flash chromatography (CH_2Cl_2, neutral alumina) to afford a dark red microcrystalline solid. Yield = 1.56 g, 57%. Melting point = 181–183 °C. ^{1}H NMR (599.5 MHz, $CDCl_3$) δ 15.34 (s, 1H, N*H*), 8.13 (d, $^3J_{HH}$ = 7 Hz, 2H, aryl C*H*), 7.79 (d, $^3J_{HH}$ = 8 Hz, 2H, aryl C*H*), 7.55 (s, 4H, aryl C*H*), 7.52−7.46 (m, 8H, aryl C*H*), 7.43−7.35 (m, 2H, aryl C*H*), 3.15 (s, 1H, alkyne C*H*). ^{13}C{^{1}H} NMR (100.6 MHz, $CDCl_3$): δ 149.6, 146.5, 141.7, 137.3, 133.6, 129.6, 129.4, 128.6, 128.0, 126.1, 120.3, 119.4,

117.4, 83.8, 78.1. FT-IR (KBr): 3280 (s), 3064 (m), 3033 (w), 2915 (m), 2849 (w), 1506 (s), 1436 (m), 1348 (m), 1313 (m), 1227 (m), 1162 (m), 1017 (m), 826 (m), 762 (s) cm^{-1}. UV-vis (CH_2Cl_2): λ_{max} = 306 nm (ε = 39,400 M^{-1} cm^{-1}), 491 nm (ε = 24,000 M^{-1} cm^{-1}). Mass Spec. (EI, +ve mode): exact mass calculated for $[C_{21}H_{16}N_4]^+$: 324.1375; exact mass found: 324.1373; difference: −0.6 ppm.

Preparation of $HC_2(BF_2L)$

$HC_2(LH)$ (2.00 g, 6.17 mmol) was dissolved in dry toluene (200 mL). NEt_3 (1.9 g, 2.6 mL, 18 mmol) was then added slowly and the solution was stirred for 10 min. $BF_3{\cdot}OEt_2$ (4.3 g, 3.8 mL, 30 mmol) was then added, and the solution was heated at 80 ºC for 18 h. The solution gradually turned from dark red to dark purple during this time. After cooling to 20 ºC, deionized H_2O (10 mL) was added to quench any excess reactive boron-containing compounds. The purple toluene solution was then washed with deionized H_2O (3 × 50 mL), dried over $MgSO_4$, gravity filtered and concentrated *in vacuo*. The resulting residue was purified by flash chromatography (CH_2Cl_2, neutral alumina) to yield a dark purple microcrystalline solid. Yield = 1.87 g, 83%. Melting point = 166−168 °C. ^{1}H NMR (399.8 MHz, $CDCl_3$) δ 8.12 (d, $^3J_{HH}$ = 7 Hz, 2H, aryl C*H*), 7.94−7.89 (m, 4H, aryl C*H*), 7.60 (d, $^3J_{HH}$ = 8 Hz, 2H, aryl C*H*), 7.53−7.43 (m, 6H, aryl C*H*), 3.24 (s, 1H, alkyne C*H*) ppm. ^{13}C NMR (100.6 MHz, $CDCl_3$): δ 144.0, 133.5, 133.0, 130.2, 129.6, 129.3, 128.9, 125.7, 123.6, 123.5, 123.2, 83.0, 80.1 ppm. ^{11}B NMR (128.3 MHz, $CDCl_3$): δ −0.6 (t, $^1J_{BF}$ = 29 Hz) ppm. ^{19}F NMR (376.1 MHz, $CDCl_3$) δ −143.6 (q, $^1J_{BF}$ = 29 Hz) ppm. FT-IR (KBr): 3066 (w), 3033 (w), 2917 (m), 2848 (m), 1507 (m), 1456 (m), 1348 (m), 1232 (s), 1148 (m), 1042 (m), 1017 (m), 764 (m) cm^{-1}. UV-vis (CH_2Cl_2): λ_{max} = 312 nm (ε = 27,400 M^{-1} cm^{-1}), 526 nm (ε = 28,300 M^{-1} cm^{-1}). Mass Spec. (EI, +ve mode): exact mass calculated for $[C_{21}H_{15}N_4BF_2]^+$: 372.1358; exact mass found: 372.1355; difference: −0.8 ppm.

Preparation of $HC_2(LH)C_2H$

In air, phenyl pyruvic acid (1.40 g, 8.53 mmol) was dissolved in 100 mL deionized H_2O containing NaOH (2.55 g, 6.38 mmol), and cooled in an ice bath. In a separate flask, 4-ethynyl aniline (2.00 g, 17.0 mmol) and concentrated hydrochloric acid (4.3 mL, 51 mmol) were mixed in deionized H_2O (15 mL) and cooled in an ice bath to 0 °C. A cooled solution of sodium nitrite (1.35 g, 20.0 mmol) in H_2O (5 mL) was then added slowly to the amine solution over a 5 min period. This mixture was stirred at 0 °C for 30 min, after which time it was added dropwise to the biphasic reaction mixture described above over a 10 min period. A dark red/purple precipitate formed almost immediately. The resulting mixture was stirred for an additional 18 h. The dark red/purple precipitate was then collected by filtration and washed with deionized H_2O (3 × 50 mL). The resulting residue was purified by flash chromatography (CH_2Cl_2, neutral alumina) to afford a dark red microcrystalline solid. Yield = 1.70 g, 57%. Melting point = 157–159 °C. ^{1}H NMR (599.5 MHz, $CDCl_3$) δ 15.28 (s, 1H, N*H*), 8.07−8.06 (m, 2H, aryl C*H*), 7.58−7.54 (m, 8H, aryl C*H*), 7.44−7.42 (m, 2H, aryl C*H*), 7.37−7.35 (m, 1H, aryl C*H*), 3.20 (s, 2H, alkyne C*H*). $^{13}C\{^1H\}$ NMR (100.6 MHz, $CDCl_3$): δ 147.8, 141.8, 137.0, 133.4, 128.5, 128.1, 126.1, 121.2, 118.8, 83.6, 78.8. FT-IR (KBr): 3276 (s), 3056 (w), 3033 (m), 2921 (m), 2852 (m), 1506 (s), 1345 (m), 1310 (w), 1224 (s), 1188 (m), 1162 (m), 1042 (m), 1018 (m), 832 (m), 768 (m) cm^{-1}. UV-vis (CH_2Cl_2): λ_{max} = 276 nm (ε = 51,200 M^{-1} cm^{-1}), 511 nm (ε = 20,500 M^{-1} cm^{-1}). Mass Spec. (EI, +ve mode): exact mass calculated for $[C_{23}H_{16}N_4]^+$: 348.1375; exact mass found: 348.1380; difference: +1.4 ppm.

Preparation of $HC_2(BF_2L)C_2H$

$HC_2(LH)C_2H$ (0.70 g, 2.0 mmol) was dissolved in dry toluene (70 mL). NEt_3 (0.61 g, 0.84 mL, 6.0 mmol) was then added slowly and the solution was stirred for 10 min. $BF_3{\cdot}OEt_2$ (1.4 g, 1.2

mL, 10. mmol) was then added, and the solution was heated at 80 ºC for 18 h. The solution gradually turned from dark red to dark purple during this time. After cooling to 20 ºC, deionized H_2O (10 mL) was added to quench any excess reactive boron-containing compounds. The purple toluene solution was then washed with deionized H_2O (3 × 50 mL), dried over $MgSO_4$, gravity filtered and concentrated *in vacuo*. The resulting residue was purified by flash chromatography (CH_2Cl_2, neutral alumina) to yield a dark purple microcrystalline solid. Yield = 0.51 g, 65%. Melting point = 162−164 °C. ^{1}H NMR (399.8 MHz, $CDCl_3$) δ 8.11−8.09 (m, 2H, aryl C*H*), 7.91 (d, $^3J_{HH}$ = 8 Hz, 4H, aryl C*H*), 7.61−7.58 (m, 4H, aryl C*H*), 7.52−7.45 (m, 3H, aryl C*H*), 3.25 (s, 2H, alkyne C*H*) ppm. ^{13}C NMR (100.6 MHz, $CDCl_3$): δ 143.9, 133.4, 133.1, 129.7, 129.0, 125.7, 123.9, 123.3, 118.8, 83.0, 80.4 ppm. ^{11}B NMR (128.3 MHz, $CDCl_3$): δ −0.6 (t, $^1J_{BF}$ = 29 Hz) ppm. ^{19}F NMR (376.1 MHz, $CDCl_3$) δ −142.9 (q, $^1J_{BF}$ = 29 Hz) ppm. FT-IR (KBr): 3065 (w), 3035 (w), 2938 (m), 2922 (m), 2857 (m), 1508 (s), 1456 (m), 1347 (m), 1301 (s), 1267 (s), 1222 (m), 1175 (m), 1119 (m), 1025 (m), 967 (s) cm^{-1}. UV-vis (CH_2Cl_2): λ_{max} = 317 nm (ε = 24,000 M^{-1} cm^{-1}), 541 nm (ε = 27,700 M^{-1} cm^{-1}). Mass Spec. (EI, +ve mode): exact mass calculated for $[C_{23}H_{15}N_4BF_2]^+$: 396.1358; exact mass found: 396.1360; difference: +0.5 ppm.

Preparation of (BF$_2$L)-(hex$_2$Fl)

HC$_2$(BF$_2$L) (0.20 g, 0.54 mmol) was mixed with **(hex$_2$Fl)N$_3$** (0.20 g, 0.54 mmol) in dry THF (6 mL). $Cu(PPh_3)_3Br$ (0.02 g, 0.03 mmol) was then added and the mixture was purged with N_2 gas for 15 min. The reaction mixture was heated with stirring at 60 °C for 18 h before it was cooled to room temperature and filtered through a small pad of neutral alumina. The resulting purple solution was concentrated *in vacuo* and the residue was purified by flash chromatography (2:1 CH_2Cl_2:hexanes, neutral alumina) to afford **(BF$_2$L)-(hex$_2$Fl)** as a dark purple solid. Yield = 0.35 g, 87%. Melting point = 63−65 °C. ^{1}H NMR (399.8 MHz, $CDCl_3$) δ 8.33 (s, 1H, triazole C*H*),

8.16−8.14 (m, 2H, aryl C*H*), 8.09−8.04 (m, 4H, aryl C*H*), 7.95−7.93 (m, 2H, aryl C*H*), 7.85−7.74 (m, 4H, aryl C*H*), 7.52−7.45 (m, 6H, aryl C*H*), 7.38−7.37 (m, 3H, aryl C*H*), 2.06−2.01 (m, 4H, alkyl C*H*), 1.13−1.02 (m, 12H, alkyl C*H*), 0.77−0.74 (m, 6H, alkyl C*H*), 0.66−0.61 (m, 4H, alkyl C*H*) ppm. ^{13}C NMR (100.6 MHz, $CDCl_3$): δ 152.9, 151.1, 149.3, 147.2, 144.0, 143.8, 142.1, 139.7, 135.9, 133.7, 131.8, 129.9, 129.5, 129.2, 128.9, 128.0, 127.2, 126.5, 125.6, 124.0, 123.6, 123.1, 120.7, 120.2, 119.4, 118.6, 115.4, 55.8, 40.5, 31.6, 29.7, 23.9, 22.7, 14.1 ppm. ^{11}B NMR (128.3 MHz, $CDCl_3$): δ −0.5 (t, $^1J_{BF}$ = 29 Hz) ppm. ^{19}F NMR (376.1 MHz, $CDCl_3$) δ −144.1 (q, $^1J_{BF}$ = 29 Hz) ppm. FT-IR (KBr): 3062 (m), 2935 (m), 2924 (m), 2851 (m), 1456 (m), 1348 (w), 1296 (m), 1268 (m), 1222 (w), 1119 (m), 964 (m), 764 (m) cm^{-1}. UV-vis (CH_2Cl_2): λ_{max} 315 nm (ε = 54,900 M^{-1} cm^{-1}), 532 nm (ε = 31,100 M^{-1} cm^{-1}). Mass Spec. (EI, +ve mode): exact mass calculated for $[C_{46}H_{48}N_7BF_2]^+$: 747.4032; exact mass found: 747.4027; difference: −0.7 ppm.

Preparation of (BF$_2$L)-(hex$_2$Fl)-(BF$_2$L)

HC$_2$(BF$_2$L) (0.15 g, 0.40 mmol) was mixed with **N$_3$(hex$_2$F)N$_3$** (0.08 g, 0.2 mmol) in dry THF (3 mL). Cu(PPh$_3$)$_3$Br (0.02 g, 0.02 mmol) was then added and the mixture was purged with N_2 gas for 15 min. The reaction mixture was heated with stirring at 60 °C for 18 h before it was cooled to room temperature and filtered through a pad of neutral alumina. The resulting purple solution was concentrated *in vacuo* and the residue was purified by flash chromatography (2:1 CH_2Cl_2:hexanes, neutral alumina) to afford **(BF$_2$L)-(hex$_2$Fl)-(BF$_2$L)** as a dark purple solid. Yield = 0.20 g, 86%. Melting point = 118−120 °C. ^{1}H NMR (399.8 MHz, $CDCl_3$) δ 8.36 (s, 2H, triazole C*H*), 8.16−8.14 (m, 4H, aryl C*H*), 8.10−8.05 (m, 8H, aryl C*H*), 7.96−7.87 (m, 8H, aryl C*H*), 7.82−7.80 (m, 2H, aryl C*H*), 7.53−7.44 (m, 12H, aryl C*H*), 2.15−2.10 (m, 4H, alkyl C*H*), 1.14−1.03 (m, 12H, alkyl C*H*), 0.77−0.74 (m, 6H, alkyl C*H*), 0.70−0.66 (m, 4H, alkyl C*H*) ppm.

^{13}C NMR (100.6 MHz, $CDCl_3$): δ 153.2, 149.2, 147.4, 144.0, 143.9, 140.6, 136.6, 133.7, 131.6, 130.0, 129.5, 129.3, 128.9, 126.6, 125.7, 124.1, 123.6, 121.3, 119.7, 118.5, 115.4, 56.4, 40.5, 31.6, 29.7, 24.0, 22.7, 14.1 ppm. ^{11}B NMR (128.3 MHz, $CDCl_3$): δ −0.5 (t, $^1J_{BF}$ = 28 Hz) ppm. ^{19}F NMR (376.1 MHz, $CDCl_3$) δ −143.7 (q, $^1J_{BF}$ = 28 Hz) ppm. FT-IR (KBr): 3065 (m), 3048 (m), 2951 (m), 2925 (s), 2852 (m), 1477 (m), 1419 (m), 1350 (m), 1296 (s), 1267 (s), 1222 (m), 1119 (m), 1007 (m), 964 (s), 845 (m), 763 (s) cm^{-1}. UV-vis (CH_2Cl_2): λ_{max} 325 nm (ε = 73, 200 M^{-1} cm^{-1}) 535 nm (ε = 51,200 M^{-1} cm^{-1}). Mass Spec. (ESI, +ve mode): exact mass calculated for $[C_{67}H_{62}N_{14}BF_2{\cdot}Na]^+$: 1183.5302; exact mass found: 1183.5309; difference: −0.6 ppm.

Preparation of (hex$_2$Fl)-(BF$_2$L)-(hex$_2$Fl)

HC$_2$(BF$_2$L)C$_2$H (0.10 g, 0.25 mmol) was mixed with **(hex$_2$Fl)N$_3$** (0.19 g, 0.50 mmol) in dry THF (4 mL). $Cu(PPh_3)_3Br$ (0.02 g, 0.03 mmol) was then added and the mixture was purged with N_2 gas for 15 min. The reaction mixture was heated with stirring at 60 °C for 18 h before it was cooled to room temperature and filtered through a pad of neutral alumina. The resulting purple solution was concentrated *in vacuo* and the residue was purified by flash chromatography (CH_2Cl_2, silica gel) to afford **(hex$_2$Fl)-(BF$_2$L)-(hex$_2$Fl)** as a dark purple solid. Yield = 0.21 g, 71%. Melting point = 77−79 °C. ^{1}H NMR (399.8 MHz, $CDCl_3$) δ 8.36 (s, 2H, triazole C*H*), 8.18 (d, $^3J_{HH}$ = 8 Hz, 2H, aryl C*H*), 8.11−8.07 (m, 8H, aryl C*H*), 7.85−7.82 (m, 4H, aryl C*H*), 7.76−7.73 (m, 4H, aryl C*H*), 7.54−7.46 (m, 3H, aryl C*H*), 7.40−7.37 (m, 6H, aryl C*H*), 2.06−2.03 (m, 8H, alkyl C*H*), 1.13−1.02 (m, 24H, alkyl C*H*), 0.76 (t, $^3J_{HH}$ = 7 Hz, 12H, alkyl C*H*), 0.68−0.63 (m, 8H, alkyl C*H*) ppm. ^{13}C NMR (100.6 MHz, $CDCl_3$): δ 152.8, 151.0, 147.2, 143.8, 142.1, 139.7, 135.9, 133.6, 131.8, 129.5, 129.5, 128.9, 128.0, 127.2, 126.5, 125.6, 124.0, 123.1, 120.7, 120.2, 119.4, 118.5, 115.4, 55.7, 40.4, 31.5, 29.7, 23.8, 22.6, 14.0 ppm. ^{11}B NMR (128.3 MHz, $CDCl_3$): δ −0.5 (t, $^1J_{BF}$ = 29 Hz) ppm. ^{19}F NMR (376.1 MHz, $CDCl_3$) δ −143.6 (q,

$^1J_{BF}$ = 29 Hz) ppm. FT-IR (KBr): 3141 (m), 3035 (m), 2938 (m), 2924 (s), 2852 (m), 1457 (s), 1299 (s), 1268 (s), 1227 (m), 1180 (m), 1122 (w), 1028 (m), 963 (s), 843 (m), 737 (m) cm^{-1}. UV-vis (CH_2Cl_2): λ_{max} 315 nm (ε = 61,600 M^{-1} cm^{-1}), 556 nm (ε = 31,100 M^{-1} cm^{-1}). Mass Spec. (ESI, +ve mode): exact mass calculated for $[C_{73}H_{81}N_{10}BF_2 \cdot Na]^+$: 1169.6604; exact mass found: 1169.6616; difference: −1.0 ppm.

Preparation of $[(BF_2L)$-$(hex_2Fl)]_n$

In a typical procedure, **$HC_2(BF_2L)C_2H$** (0.13 g, 0.34 mmol) was mixed with **$N_3(hex_2F)N_3$** (0.14 g, 0.34 mmol) in dry THF (3 mL). $Cu(PPh_3)_3Br$ (0.02 g, 0.02 mmol) was then added and the mixture was purged with N_2 for 15 min. The reaction mixture was heated with stirring at 60 °C for 48 h before it was cooled to room temperature and filtered through a pad of neutral alumina. The resulting solution was added to cold hexanes to precipitate **$[(BF_2L)$-$(hex_2Fl)]_n$** as a dark purple solid. The precipitation was repeated two additional times. Yield = 0.26 g, 94%. ^{1}H NMR (399.8 MHz, $CDCl_3$) δ 8.38−8.30 (m, 2H, triazole C*H*), 8.18−8.07 (m, 5H, aryl C*H*), 7.94−7.80 (m, 5H, aryl C*H*), 7.70−7.47 (m, 9H, aryl C*H*), 2.13−1.82 (m, 6H, alkyl C*H*), 1.13−0.97 (m, 10H, alkyl C*H*), 0.80−0.69 (m, 8H, alkyl C*H*), 0.49 (br s, 2H, alkyl C*H*) ppm. ^{11}B NMR (128.3 MHz, $CDCl_3$): δ −0.5 (br s) ppm. ^{19}F NMR (376.1 MHz, $CDCl_3$) δ −143.4 (br s) ppm. FT-IR (KBr): 3057 (m), 2936 (m), 2924 (s), 2852 (s), 1473 (m), 1436 (m), 1346 (m), 1299 (m), 1268 (m), 1222 (m), 1176 (m), 1119 (m), 1007 (m), 963 (m), 842 (m), 720 (m) cm^{-1}. UV-vis (DMF): λ_{max} 330 nm (ε = 45, 700 M^{-1} cm^{-1}), 559 nm (ε = 25, 700 M^{-1} cm^{-1}). GPC (DMF, conventional calibration *vs.* PS standards): M_n = 17,000 g mol^{-1}, M_w = 32,750 g mol^{-1}, $Đ$ = 2.14.

Molecular Weight of $[(BF_2L)$-$(hex_2Fl)]_n$ as a Function of Reaction Time

In a typical procedure, **$HC_2(BF_2L)C_2H$** (0.119 g, 0.30 mmol) was mixed with **$N_3(hex_2F)N_3$** (0.125 g, 0.30 mmol) in dry THF (3 mL). $Cu(PPh_3)_3Br$ (0.014 g, 0.015 mmol) was then added,

and the mixture was purged with N_2 for 15 min. The reaction mixture was heated with stirring at 60 °C. Aliquots (0.5 mL) were removed from the reactions at 12, 24, 48, 72 and 168 h. All aliquots were filtered through a pad of neutral alumina. The resulting solution was added to cold hexanes to precipitate **[(BF$_2$L)-(hex$_2$Fl)]$_n$** as a dark purple solid. The precipitation was repeated two additional times. The degree of polymerization was determined by GPC analysis in DMF (conventional calibration vs. polystyrene).

Acknowledgements

We would like to thank the University of Western Ontario, the Natural Science and Engineering Research Council (NSERC) of Canada (J. B. G.: DG, 435675 and S. M. B.,: CGS M and CGS D scholarships), the Ontario Ministry of Research and Innovation (J. B. G.: ERA, ER14-10-147) and the Canada Foundation for Innovation (J. B. G.: JELF, 33977) for funding this work. Finally, we thank Prof. Elizabeth R. Gillies, Prof. Mark S. Workentin, and the Western Nanofabrication Facility for access to instrumentation.

References

1. N. Matsumi and Y. Chujo, *Polym. J.*, 2008, **40**, 77−89.
2. F. Jäkle, *Chem. Rev.*, 2010, **110**, 3985−4022.
3. V. R. Donuru, G. K. Vegesna, S. Velayudham, S. Green and H. Liu, *Chem. Mater.*, 2009, **21**, 2130−2138.
4. H. Li and F. Jäkle, *Angew. Chem. Int. Ed.*, 2009, **48**, 2313−2316.
5. Y. Tokoro, A. Nagai, K. Kokado and Y. Chujo, *Macromolecules*, 2009, **42**, 2988−2993.
6. N. Matsumi, K. Kawaguchi, Y. Hirota and K. Aoi, *J. Organomet. Chem.*, 2009, **694**, 1776−1779.
7. H. Li and F. Jäkle, *Macromol. Rapid Commun.*, 2010, **31**, 915−920.

8. A. Nagai and Y. Chujo, *Macromolecules*, 2010, **43**, 193−200.

9. L. Gao, W. Senevirathna and G. Sauvé, *Org. Lett.*, 2011, **13**, 5354−5357.

10. B. C. Popere, A. M. Della Pelle and S. Thayumanavan, *Macromolecules*, 2011, **44**, 4767−4776.

11. A. B. Nepomnyashchii, M. Bröring, J. Ahrens and A. J. Bard, *J. Am. Chem. Soc.*, 2011, **133**, 8633−8645.

12. B. C. Popere, A. M. Della Pelle, A. Poe, G. Balaji and S. Thayumanavan, *Chem. Sci.*, 2012, **3**, 3093−3102.

13. X. Ma, X. Mao, S. Zhang, X. Huang, Y. Cheng and C. Zhu, *Polym. Chem.*, 2013, **4**, 520−527.

14. R. Yoshii, A. Hirose, K. Tanaka and Y. Chujo, *J. Am. Chem. Soc.*, 2014, **136**, 18131−18139.

15. R. Vedarajan, Y. Hosono and N. Matsumi, *Solid State Ionics*, 2014, **262**, 795−800.

16. A. W. Baggett, F. Guo, B. Li, S.-Y. Liu and F. Jäkle, *Angew. Chem. Int. Ed.*, 2015, **54**, 11191−11195.

17. X. Yin, F. Guo, R. A. Lalancette and F. Jäkle, *Macromolecules*, 2016, **49**, 537−546.

18. F. Cheng, E. M. Bonder and F. Jäkle, *J. Am. Chem. Soc.*, 2013, **135**, 17286−17289.

19. Z. Zhang, R. M. Edkins, J. Nitsch, K. Fucke, A. Eichhorn, A. Steffen, Y. Wang and T. B. Marder, *Chem. Eur. J.*, 2015, **21**, 177−190.

20. G. Zhang, G. M. Palmer, M. W. Dewhirst and C. L. Fraser, *Nat. Mater.*, 2009, **8**, 747−751.

21. T. Kim, S. Lim, S.-R. Park, C. J. Han and M. H. Lee, *Polymer*, 2015, **66**, 67−75.

22. B. H. Lessard, K. L. Sampson, T. Plint and T. P. Bender, *J. Polym. Sci. Part A: Polym. Chem.*, 2015, **53**, 1996−2006.

23. S. R. Shankar and N. Matsumi, *Polym. Bull.*, 2012, **68**, 721−727.

24. S. Cataldo, S. Fabiano, F. Ferrante, F. Previti, S. Patanè and B. Pignataro, *Macromol. Rapid Commun.*, 2010, **31**, 1281−1286.

25. N. Matsumi, K. Naka and Y. Chujo, *J. Am. Chem. Soc.*, 1998, **120**, 5112−5113.

26. N. Matsumi, K. Naka and Y. Chujo, *Macromolecules*, 1998, **31**, 8047−8050.

27. Y. Qin, C. Pagba, P. Piotrowiak and F. Jäkle, *J. Am. Chem. Soc.*, 2004, **126**, 7015−7018.

28. D. Reitzenstein and C. Lambert, *Macromolecules*, 2009, **42**, 773−782.

29. A. Pfister, G. Zhang, J. Zareno, A. F. Horwitz and C. L. Fraser, *ACS Nano*, 2008, **2**, 1252−1258.

30. C. Thivierge, A. Loudet and K. Burgess, *Macromolecules*, 2011, **44**, 4012−4015.

31. C. Dai, D. Yang, X. Fu, Q. Chen, C. Zhu, Y. Cheng and L. Wang, *Polym. Chem.*, 2015, **6**, 5070−5076.

32. F. R. Kersey, G. Zhang, G. M. Palmer, M. W. Dewhirst and C. L. Fraser, *ACS Nano*, 2010, **4**, 4989−4996.

33. S. Novoa, J. A. Paquette, S. M. Barbon, R. R. Maar and J. B. Gilroy, *J. Mater. Chem. C*, 2016, DOI: 10.1039/C1035TC03287C.

34. D. A. Brown, H. Bögge, G. N. Lipunova, A. Müller, W. Plass and K. G. Walsh, *Inorg. Chim. Acta*, 1998, **280**, 30−38.

35. J. B. Gilroy, B. O. Patrick, R. McDonald and R. G. Hicks, *Inorg. Chem.*, 2008, **47**, 1287−1294.

36. M.-C. Chang and E. Otten, *Chem. Commun.*, 2014, **50**, 7431−7433.

37. M.-C. Chang, T. Dann, D. P. Day, M. Lutz, G. G. Wildgoose and E. Otten, *Angew. Chem. Int. Ed.*, 2014, **53**, 4118−4122.

38. S. M. Barbon, P. A. Reinkeluers, J. T. Price, V. N. Staroverov and J. B. Gilroy, *Chem. Eur. J.*, 2014, **20**, 11340−11344.

39. S. M. Barbon, J. T. Price, P. A. Reinkeluers and J. B. Gilroy, *Inorg. Chem.*, 2014, **53**, 10585−10593.

40. R. Travieso-Puente, M.-C. Chang and E. Otten, *Dalton Trans.*, 2014, **43**, 18035−18041.

41. M.-C. Chang, P. Roewen, R. Travieso-Puente, M. Lutz and E. Otten, *Inorg. Chem.*, 2015, **54**, 379−388.

42. A. Mandal, B. Schwederski, J. Fiedler, W. Kaim and G. K. Lahiri, *Inorg. Chem.*, 2015, **54**, 8126−8135.

43. W. Schorn, D. Grosse-Hagenbrock, B. Oelkers and J. Sundermeyer, *Dalton Trans.*, 2016, **45**, 1201−1207.

44. E. Kabir, C.-H. Wu, J. I.-C. Wu and T. S. Teets, *Inorg. Chem.*, 2016, **55**, 956−963.

45. M.-C. Chang and E. Otten, *Organometallics*, 2016, **35**, 534−542.

46. R. R. Maar, S. M. Barbon, N. Sharma, H. Groom, L. G. Luyt and J. B. Gilroy, *Chem. Eur. J.*, 2015, **21**, 15589−15599.

47. M.-C. Chang and E. Otten, *Inorg. Chem.*, 2015, **54**, 8656−8664.

48. M. Hesari, S. M. Barbon, V. N. Staroverov, Z. Ding and J. B. Gilroy, *Chem. Commun.*, 2015, **51**, 3766−3769.

49. S. M. Barbon, V. N. Staroverov and J. B. Gilroy, *J. Org. Chem.*, 2015, **80**, 5226−5235.

50. A. Qin, J. W. Y. Lam and B. Z. Tang, *Chem. Soc. Rev.*, 2010, **39**, 2522−2544.

51. A. Qin, J. W. Y. Lam and B. Z. Tang, *Macromolecules*, 2010, **43**, 8693−8702.

52. P. Wu, A. K. Feldman, A. K. Nugent, C. J. Hawker, A. Scheel, B. Voit, J. Pyun, J. M. J. Fréchet, K. B. Sharpless and V. V. Fokin, *Angew. Chem. Int. Ed.*, 2004, **43**, 3928−3932.

53. A. J. Scheel, H. Komber and B. I. Voit, *Macromol. Rapid Commun.*, 2004, **25**, 1175−1180.

54. S. Srinivasachari, Y. Liu, G. Zhang, L. Prevette and T. M. Reineke, *J. Am. Chem. Soc.*, 2006, **128**, 8176−8184.

55. A. Qin, J. W. Y. Lam, C. K. W. Jim, L. Zhang, J. Yan, M. Häussler, J. Liu, Y. Dong, D. Liang, E. Chen, G. Jia and B. Z. Tang, *Macromolecules*, 2008, **41**, 3808−3822.

56. M. A. Karim, Y.-R. Cho, J. S. Park, S. C. Kim, H. J. Kim, J. W. Lee, Y.-S. Gal and S.-H. Jin, *Chem. Commun.*, 2008, 1929−1931.

57. R. Westlund, E. Glimsdal, M. Lindgren, R. Vestberg, C. Hawker, C. Lopes and E. Malmström, *J. Mater. Chem.*, 2008, **18**, 166−175.

58. M. Albrecht, A. Lippach, M. P. Exner, J. Jerbi, M. Springborg, N. Budisa and G. Wenz, *Org. Biomol. Chem.*, 2015, **13**, 6728−6736.

59. K. Suzuki, A. Kobayashi, S. Kaneko, K. Takehira, T. Yoshihara, H. Ishida, Y. Shiina, S. Oishi and S. Tobita, *Phys. Chem. Chem. Phys.*, 2009, **11**, 9850−9860.

60. S. Fery-Forgues and D. Lavabre, *J. Chem. Educ.*, 1999, **76**, 1260−1264.

61. J. B. Gilroy, M. J. Ferguson, R. McDonald, B. O. Patrick and R. G. Hicks, *Chem. Commun.*, 2007, 126−128.

62. C. M. Cardona, W. Li, A. E. Kaifer, D. Stockdale and G. C. Bazan, *Adv. Mater.*, 2011, **23**, 2367−2371.

63. D. J. V. C. van Steenis, O. R. P. David, G. P. F. van Strijdonck, J. H. van Maarseveen and J. N. H. Reek, *Chem. Commun.*, 2005, 4333−4335.

64. S. Barik, S. Friedland and W. G. Skene, *Can. J. Chem.*, 2010, **88**, 945−953.

65. J. B. Gilroy, S. D. J. McKinnon, B. D. Koivisto and R. G. Hicks, *Org. Lett.*, 2007, **9**, 4837−4840.

Supplementary Information

Boron Difluoride Formazanate Copolymers with 9,9-Di-*n*-hexylfluorene Prepared by Copper Catalyzed Alkyne-Azide Cycloaddition Chemistry

*Stephanie M. Barbon and Joe B. Gilroy**

Department of Chemistry and the Centre for Advanced Materials and Biomaterials Research (CAMBR), The University of Western Ontario, 1151 Richmond St. N., London, Ontario, Canada, N6A 5B7. Tel: +1-519-661-2111 ext. 81561; E-mail: joe.gilroy@uwo.ca

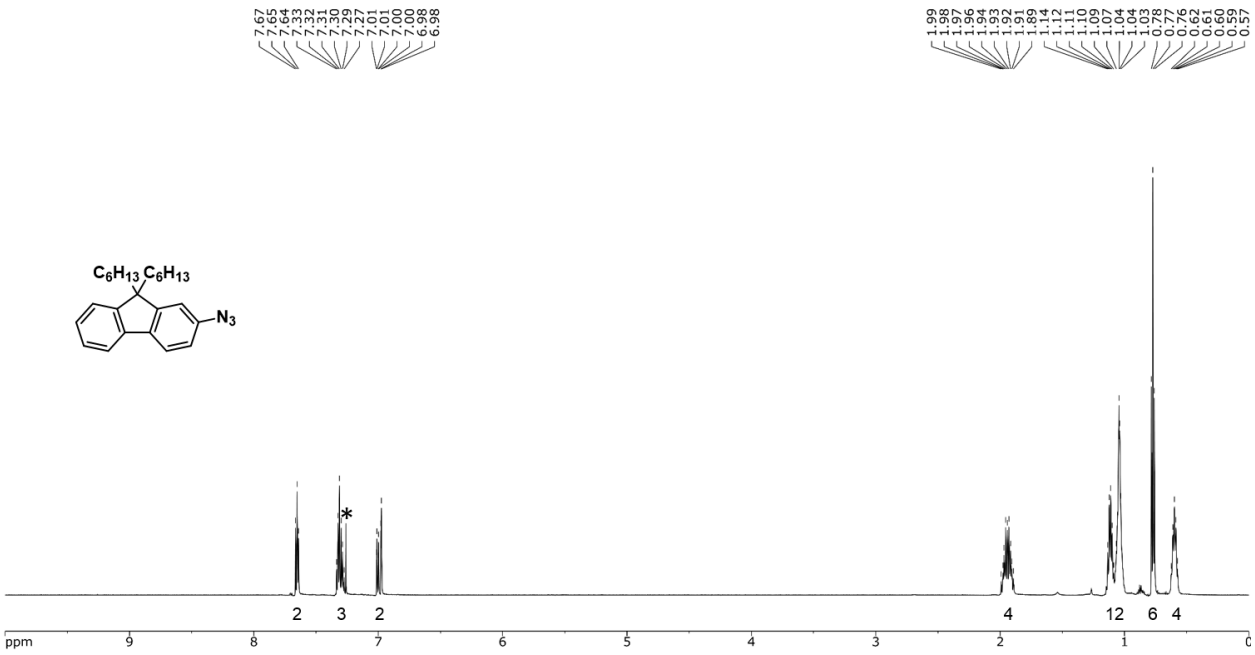

Fig. S1 ^{1}H NMR spectrum of **(hex$_2$Fl)N$_3$** in $CDCl_3$. The asterisk denotes residual solvent signal.

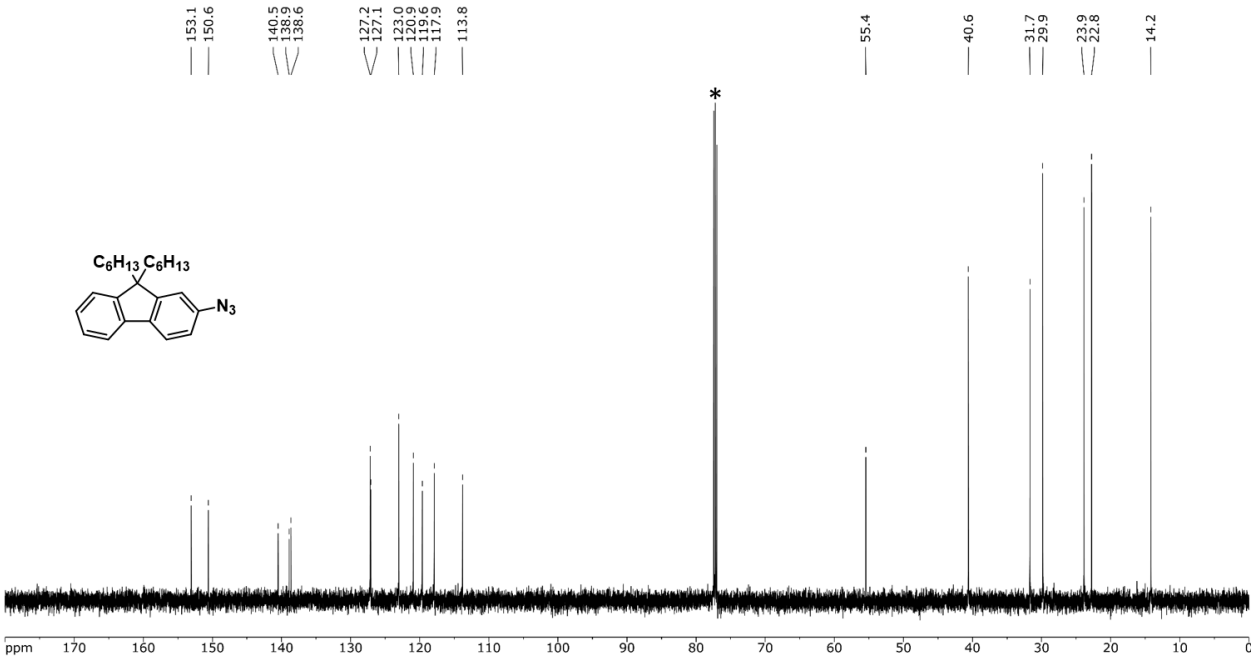

Fig. S2 $^{13}C\{^{1}H\}$ NMR spectrum of **(hex$_2$Fl)N$_3$** in $CDCl_3$. The asterisk denotes solvent signal.

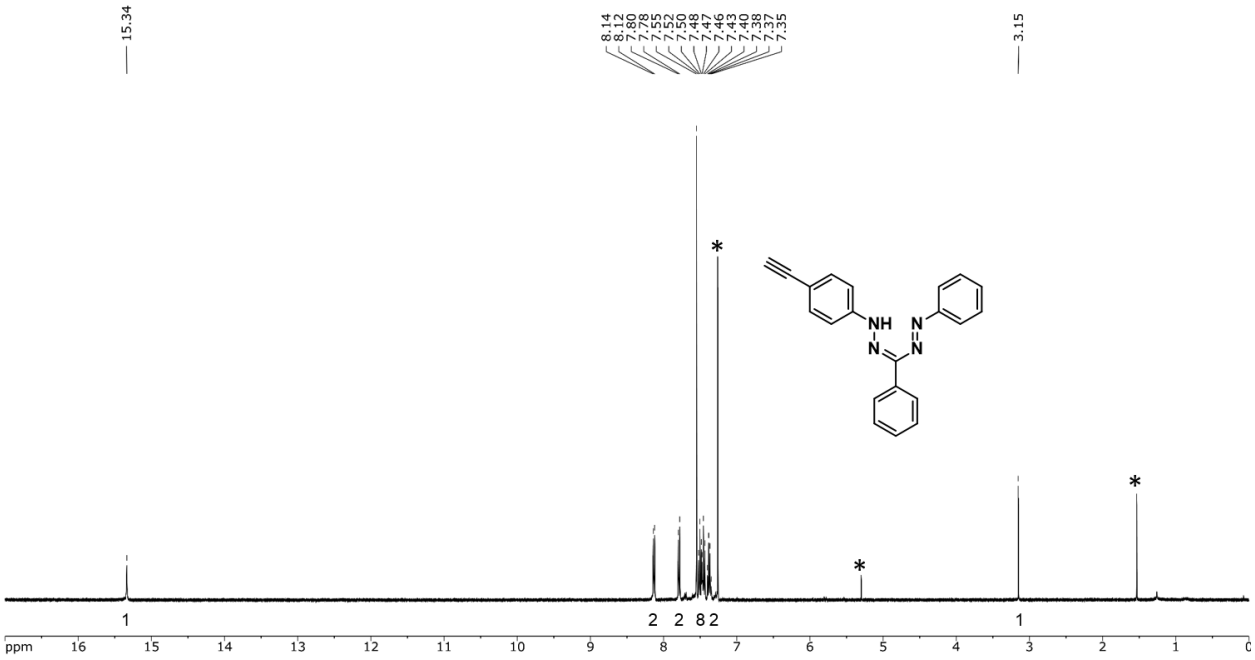

Fig. S3 ^{1}H NMR spectrum of **HC_2(LH)** in $CDCl_3$. The asterisks denote residual solvent signals.

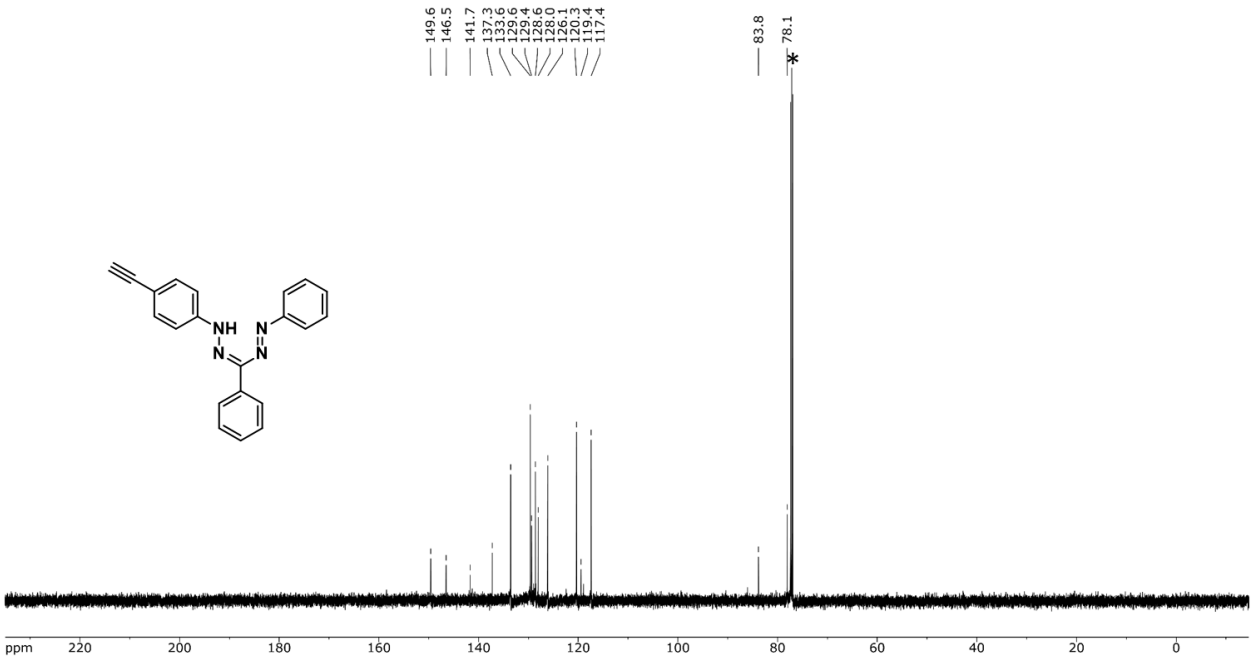

Fig. S4 $^{13}C\{^{1}H\}$ NMR spectrum of **HC_2(LH)** in $CDCl_3$. The asterisk denotes solvent signal.

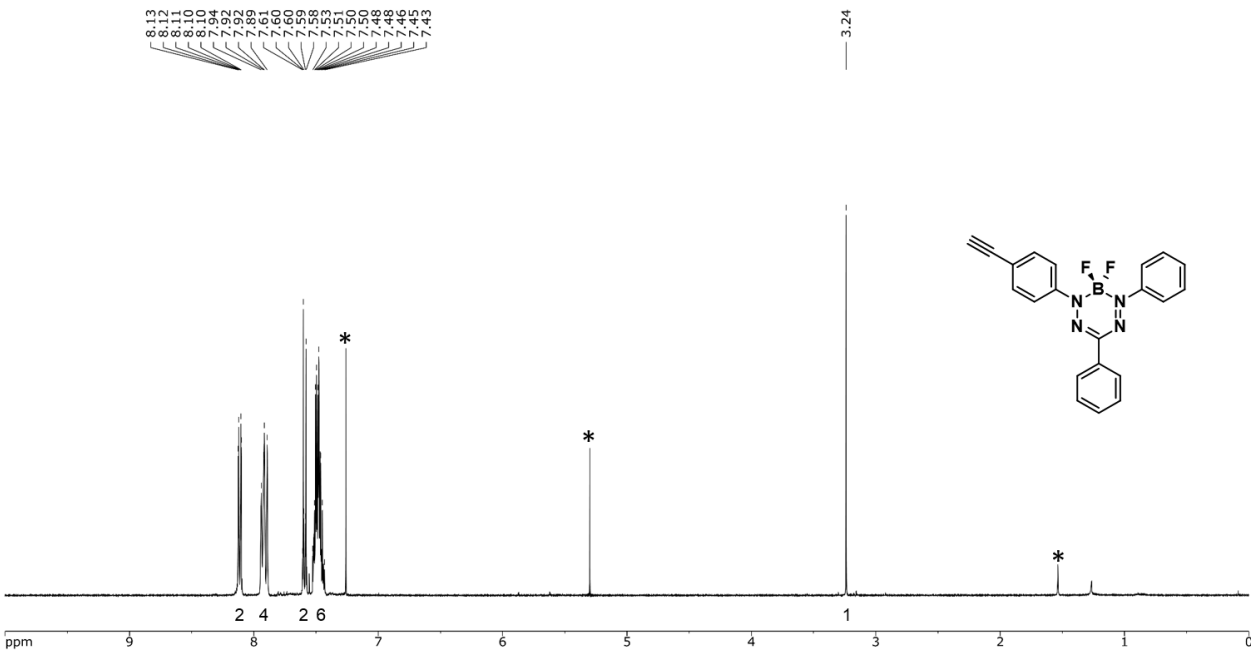

Fig. S5 ^{1}H NMR spectrum of **$HC_2(BF_2L)$** in $CDCl_3$. The asterisks denote residual solvent signals.

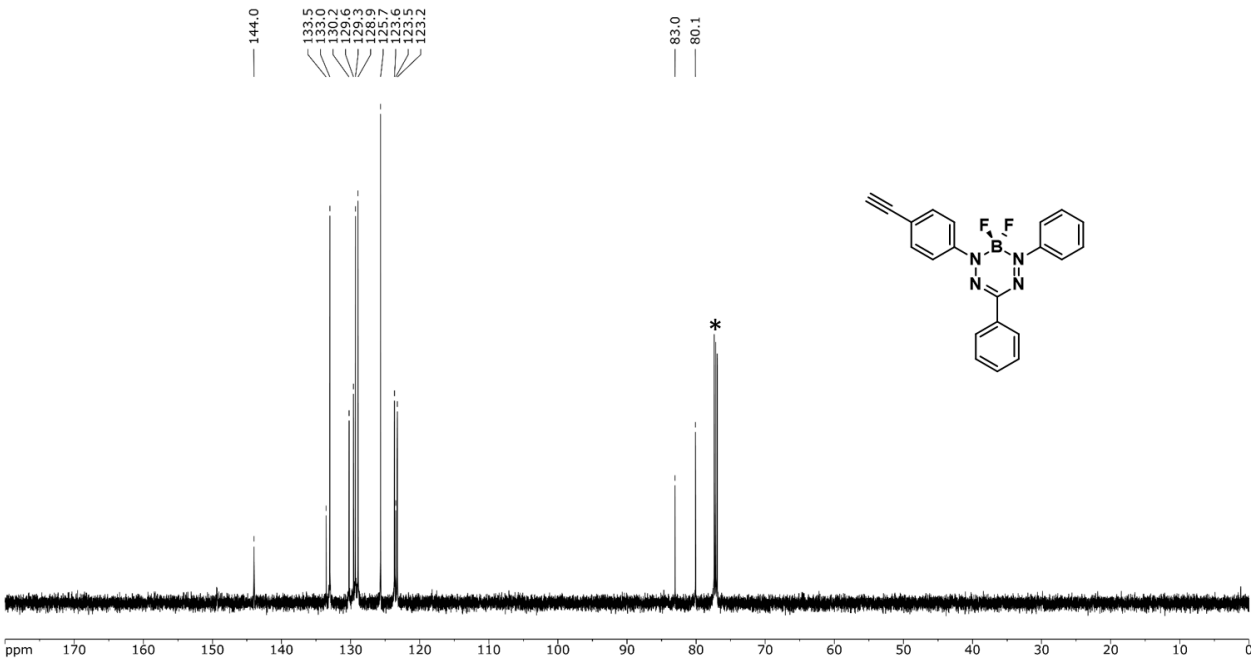

Fig. S6 $^{13}C\{^{1}H\}$ NMR spectrum of **$HC_2(BF_2L)$** in $CDCl_3$. The asterisk denotes solvent signal.

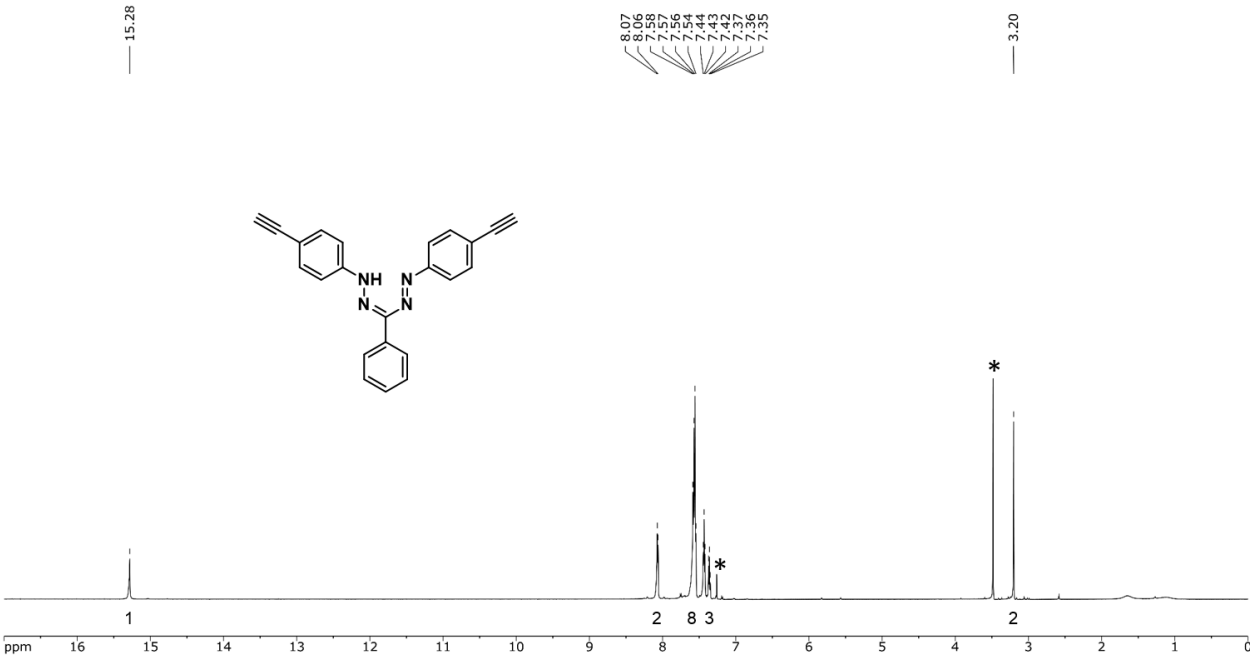

Fig. S7 ^{1}H NMR spectrum of **$HC_2(LH)C_2H$** in $CDCl_3$. The asterisks denote residual solvent signals.

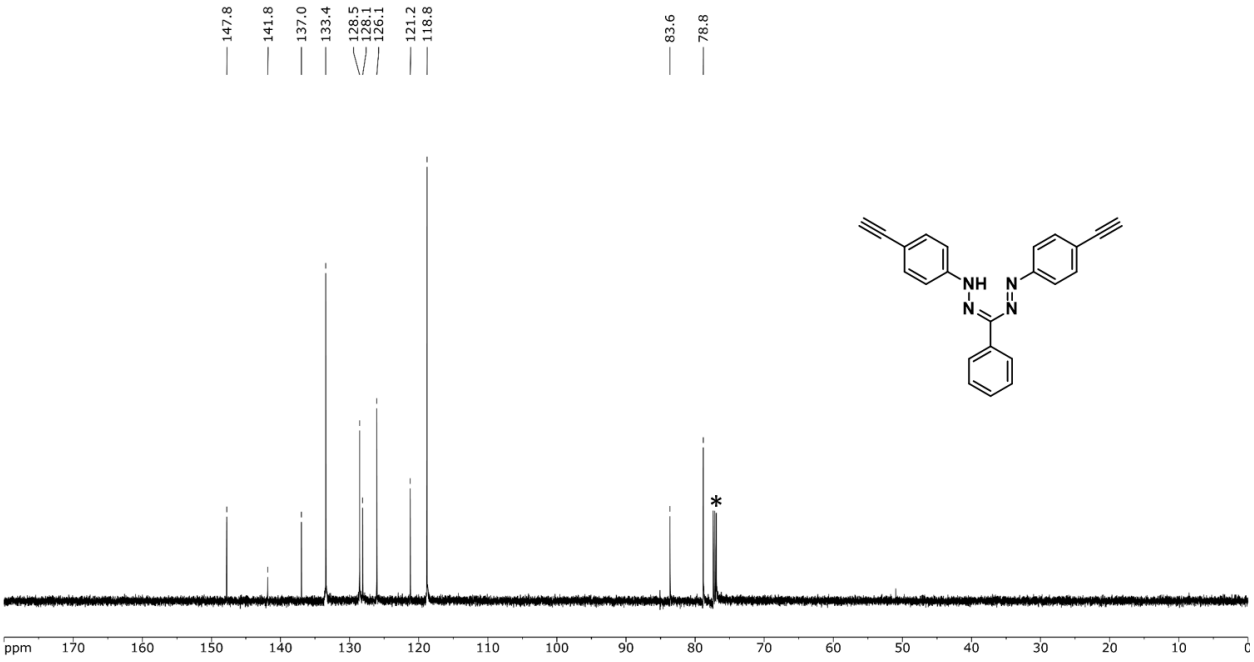

Fig. S8 $^{13}C\{^{1}H\}$ NMR spectrum of **$HC_2(LH)C_2H$** in $CDCl_3$. The asterisk denotes solvent signal.

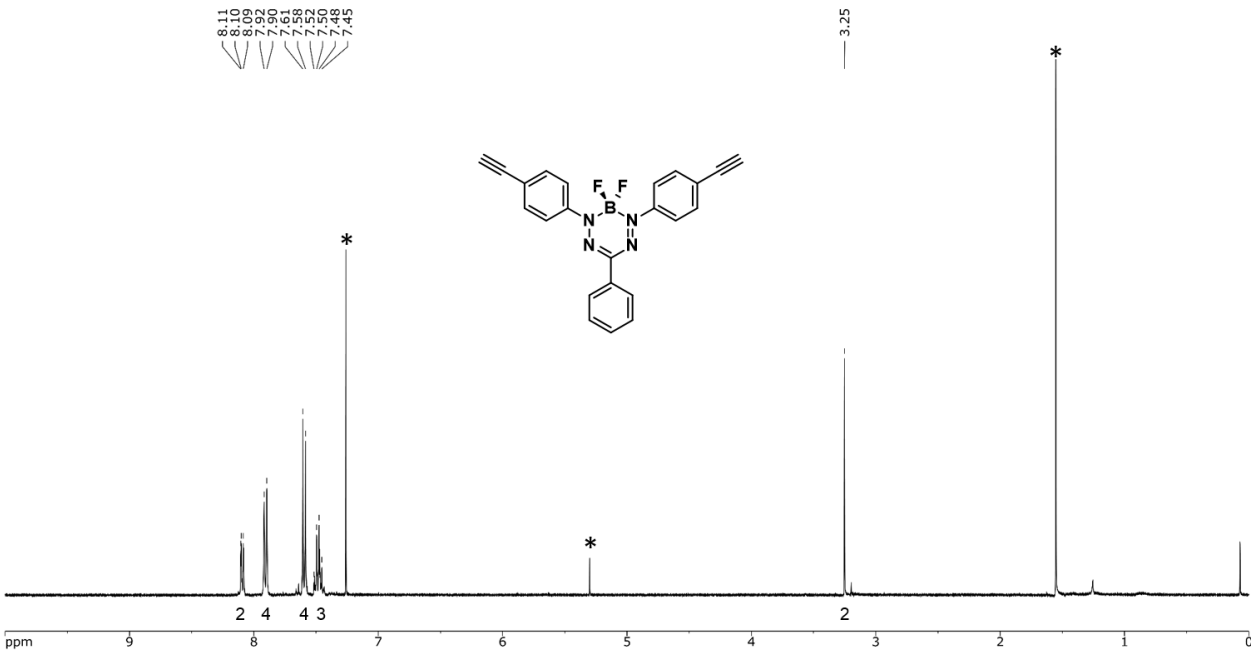

Fig. S9 ^{1}H NMR spectrum of **$HC_2(BF_2L)C_2H$** in $CDCl_3$. The asterisks denote residual solvent signals.

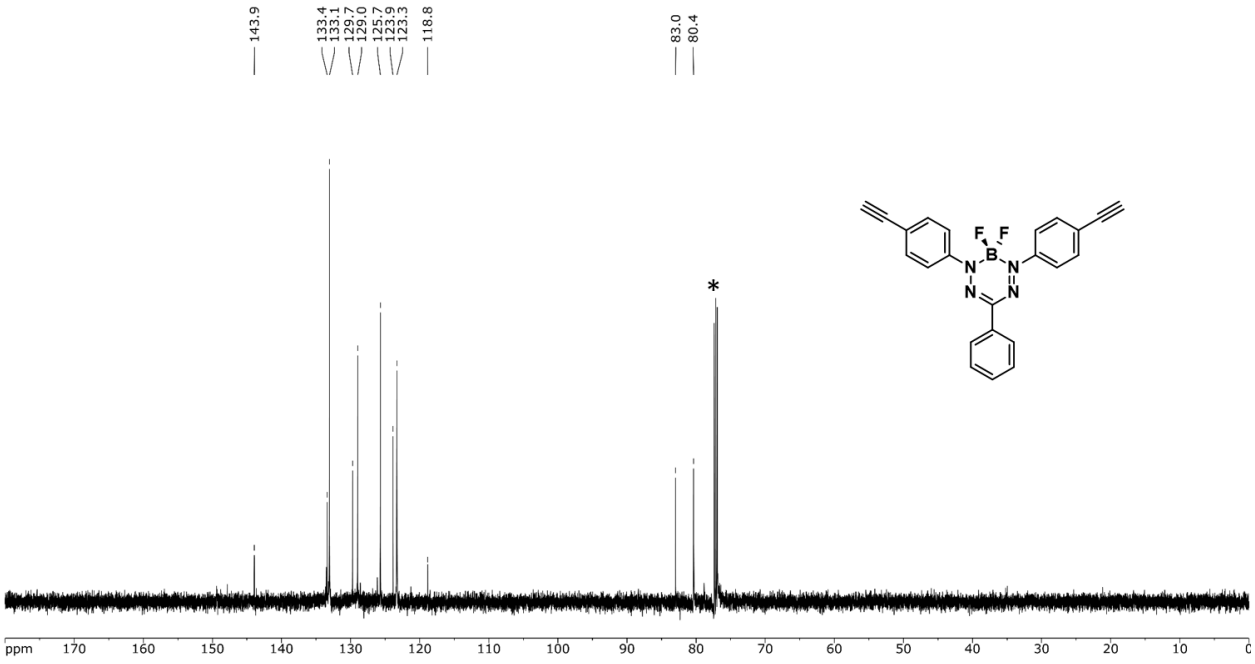

Fig. S10 $^{13}C\{^{1}H\}$ NMR spectrum of **$HC_2(BF_2L)C_2H$** in $CDCl_3$. The asterisk denotes solvent signal.

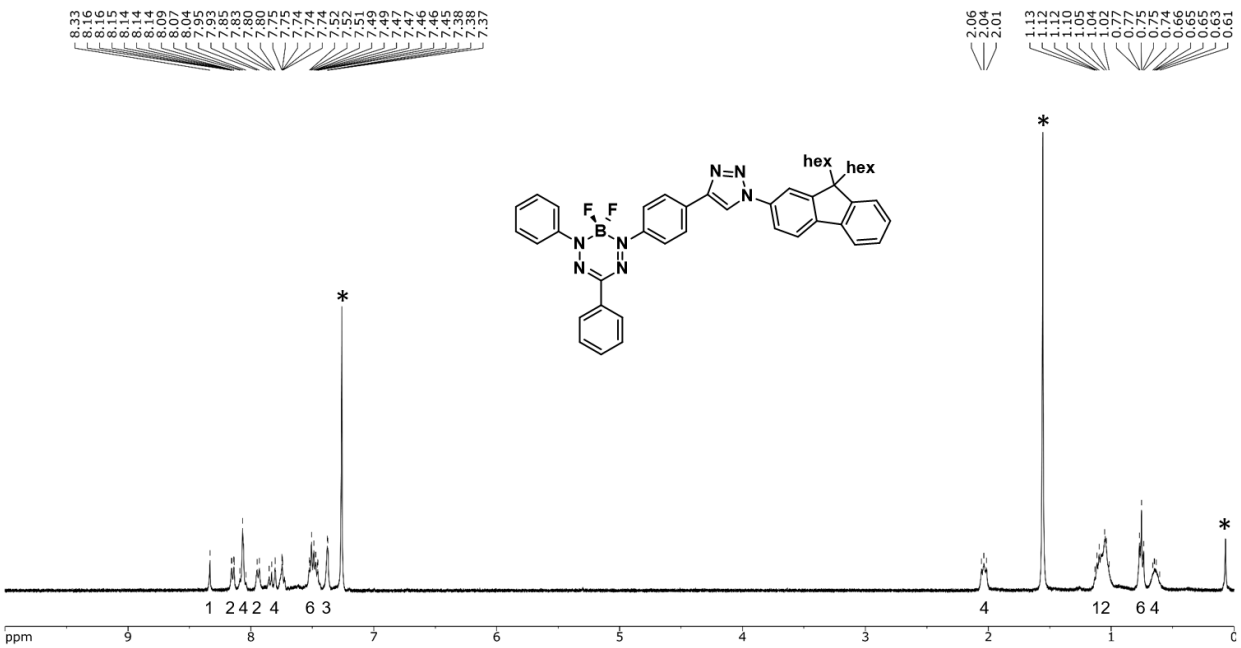

Fig. S11 ^{1}H NMR spectrum of **(BF_2L)-(hex$_2$Fl)** in $CDCl_3$. The asterisks denote residual solvent or grease signals.

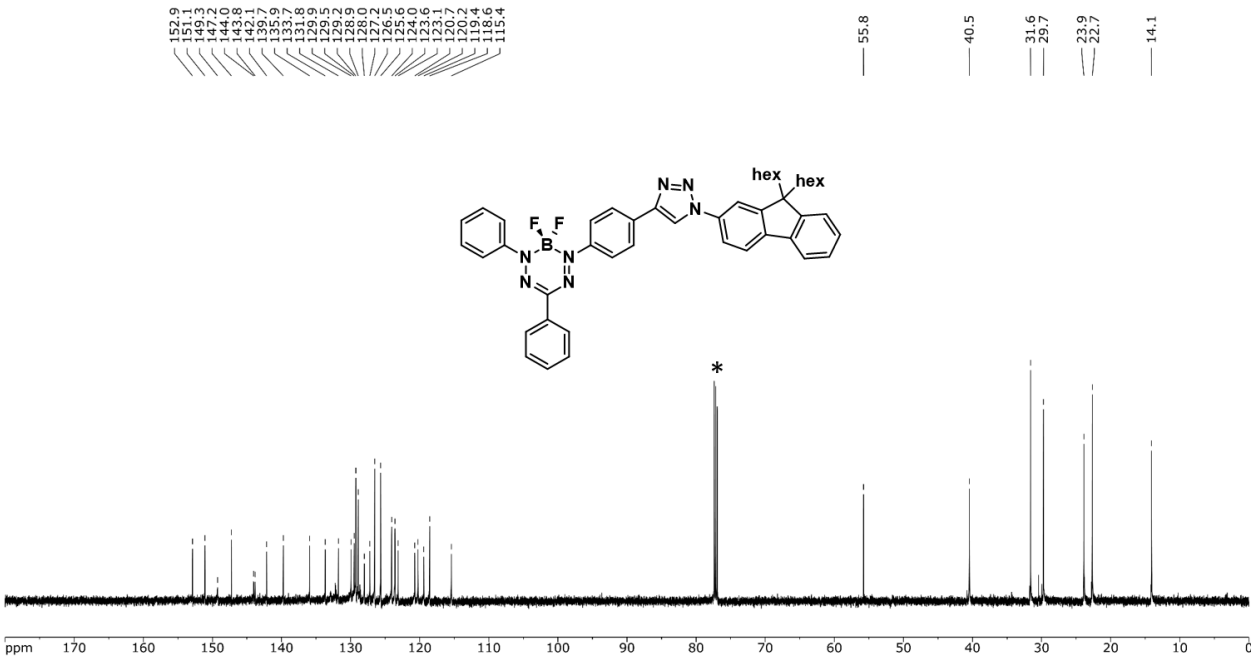

Fig. S12 $^{13}C\{^{1}H\}$ NMR spectrum of **(BF_2L)-(hex$_2$Fl)** in $CDCl_3$. The asterisk denotes solvent signal.

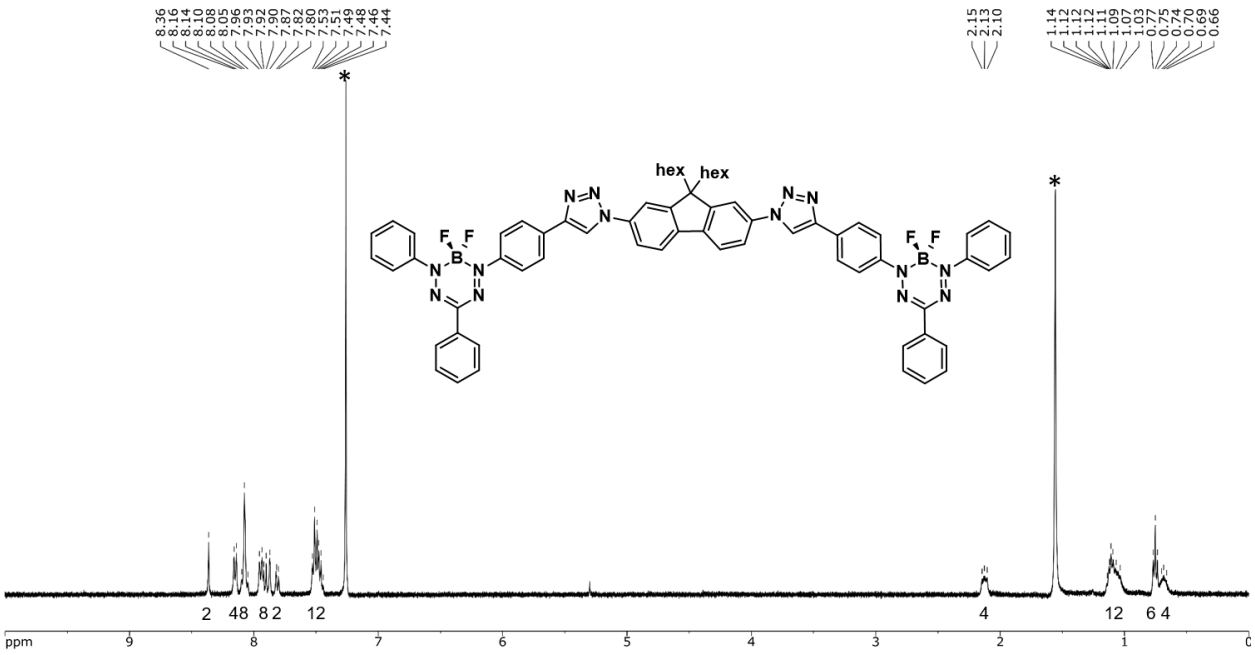

Fig. S13 ^{1}H NMR spectrum of **(BF$_2$L)-(hex$_2$Fl)-(BF$_2$L)** in $CDCl_3$. The asterisks denote residual solvent signals.

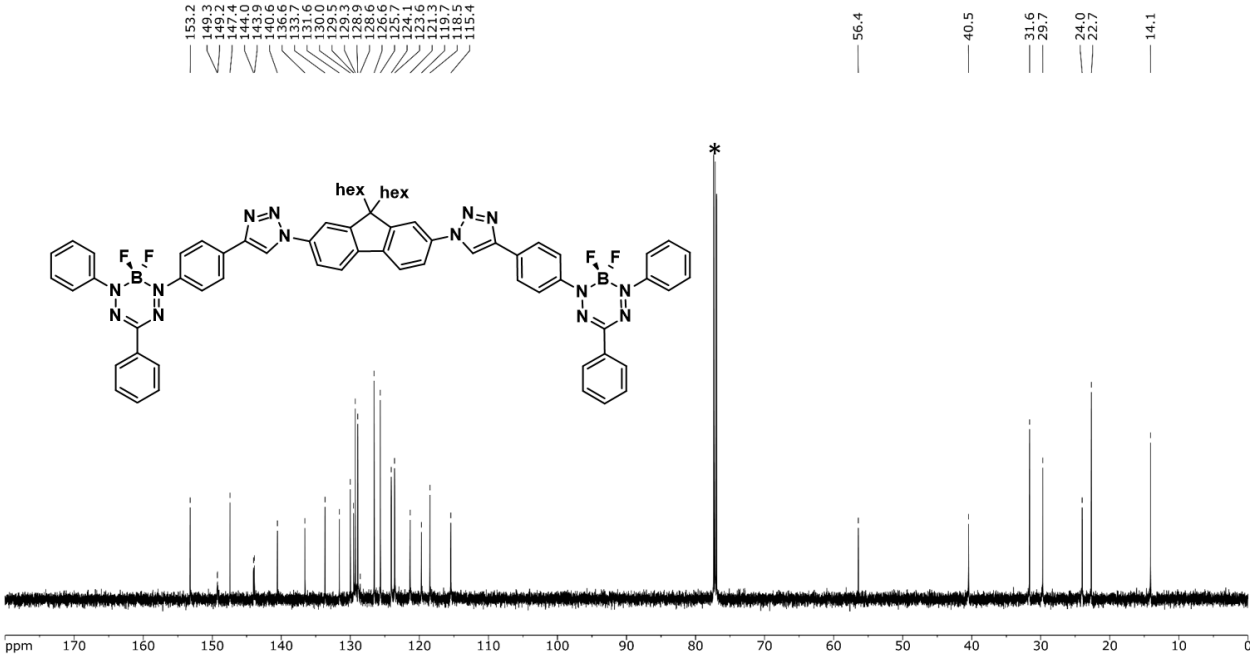

Fig. S14 $^{13}C\{^{1}H\}$ NMR spectrum of **(BF$_2$L)-(hex$_2$Fl)-(BF$_2$L)** in $CDCl_3$. The asterisk denotes solvent signal.

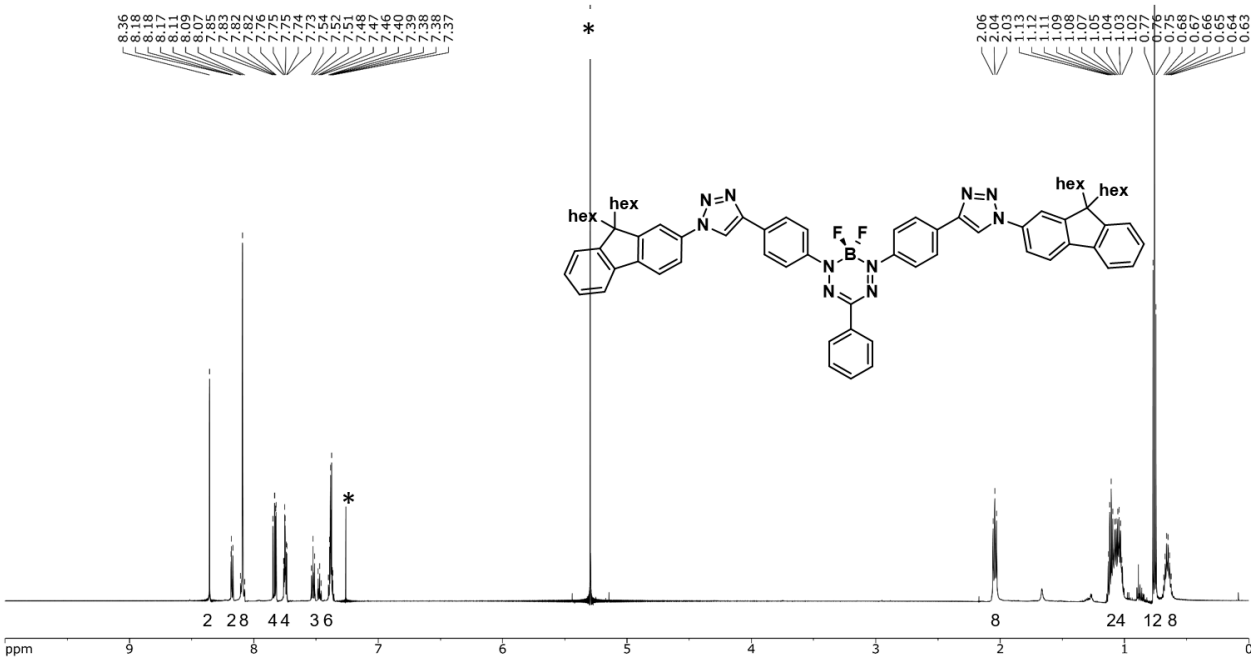

Fig. S15 ^{1}H NMR spectrum of **(hex$_2$Fl)-(BF$_2$L)-(hex$_2$Fl)** in $CDCl_3$. The asterisks denote residual solvent signals.

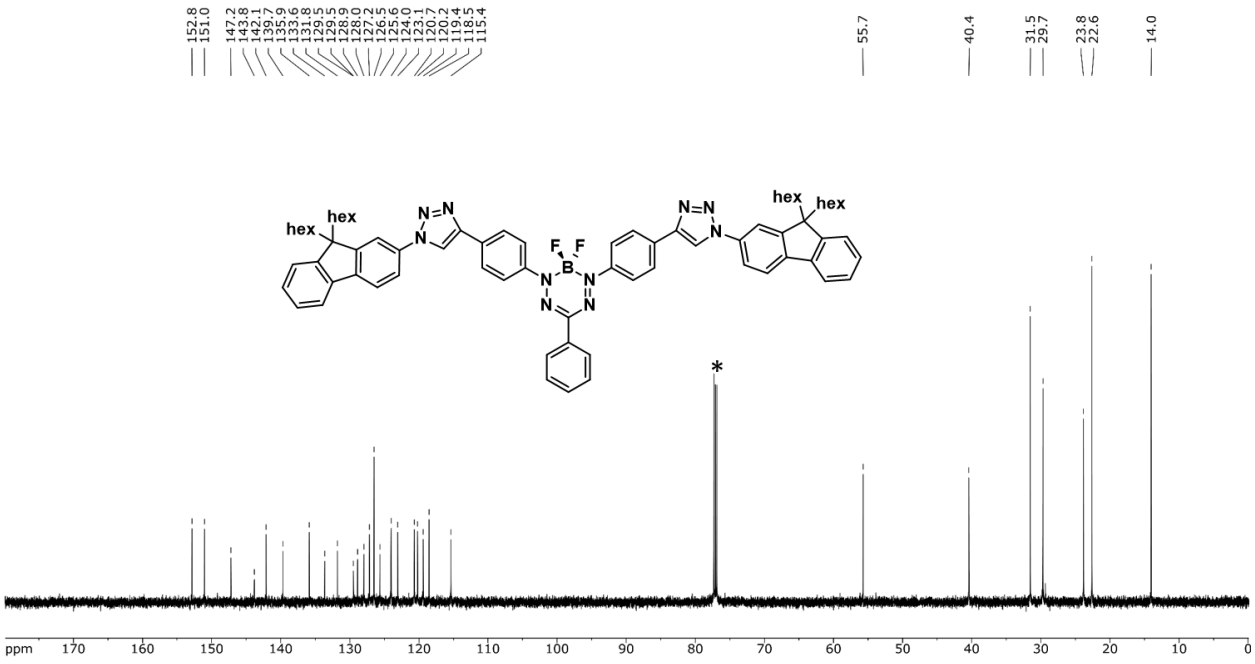

Fig. S16 $^{13}C\{^{1}H\}$ NMR spectrum of **(hex$_2$Fl)-(BF$_2$L)-(hex$_2$Fl)** in $CDCl_3$. The asterisk denotes solvent signal.

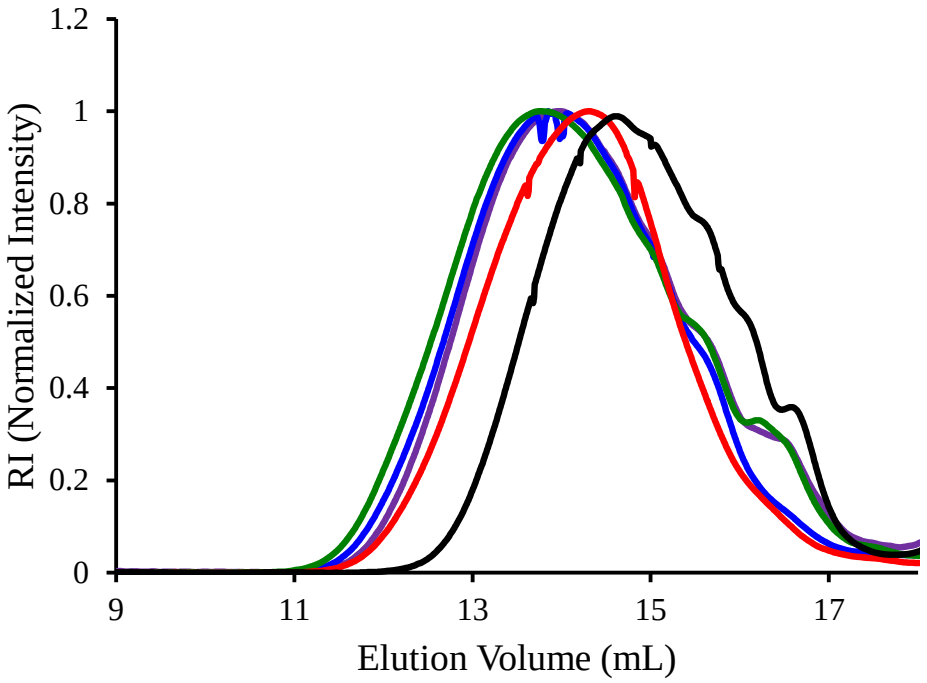

Fig. S17 GPC traces for aliquots of polymer **[(BF$_2$L)-(hex$_2$Fl)]$_n$** taken at 12 h (black), 24 h (purple), 48 h (blue), 72 h (green) and 168 h (red).

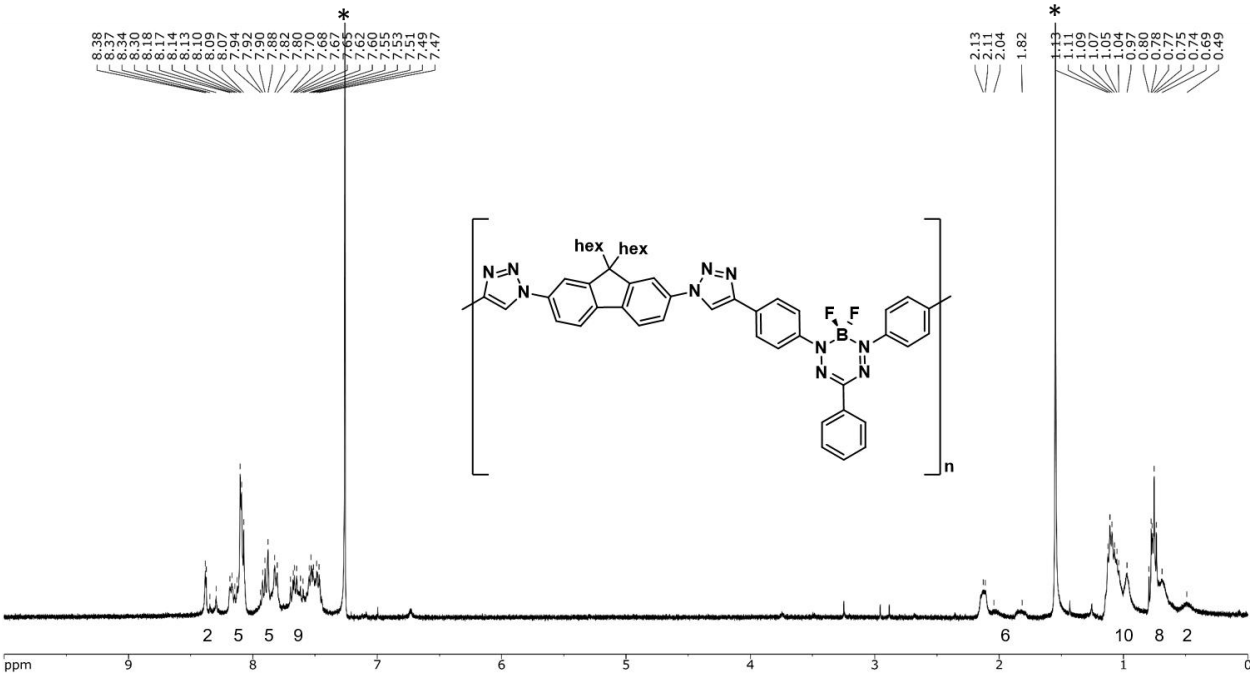

Fig. S18 ^{1}H NMR spectrum of **[(BF$_2$L)-(hex$_2$Fl)]$_n$** in $CDCl_3$. The asterisks denote residual solvent signals.

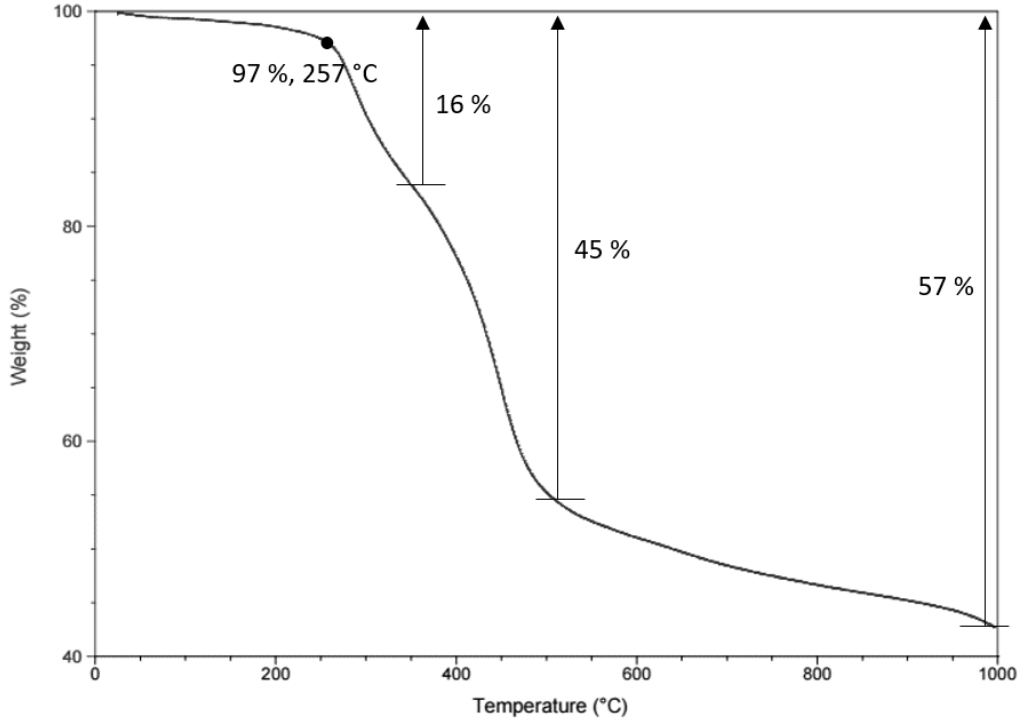

Fig. S19 TGA trace for **[(BF$_2$L)-(hex$_2$Fl)]$_n$**.

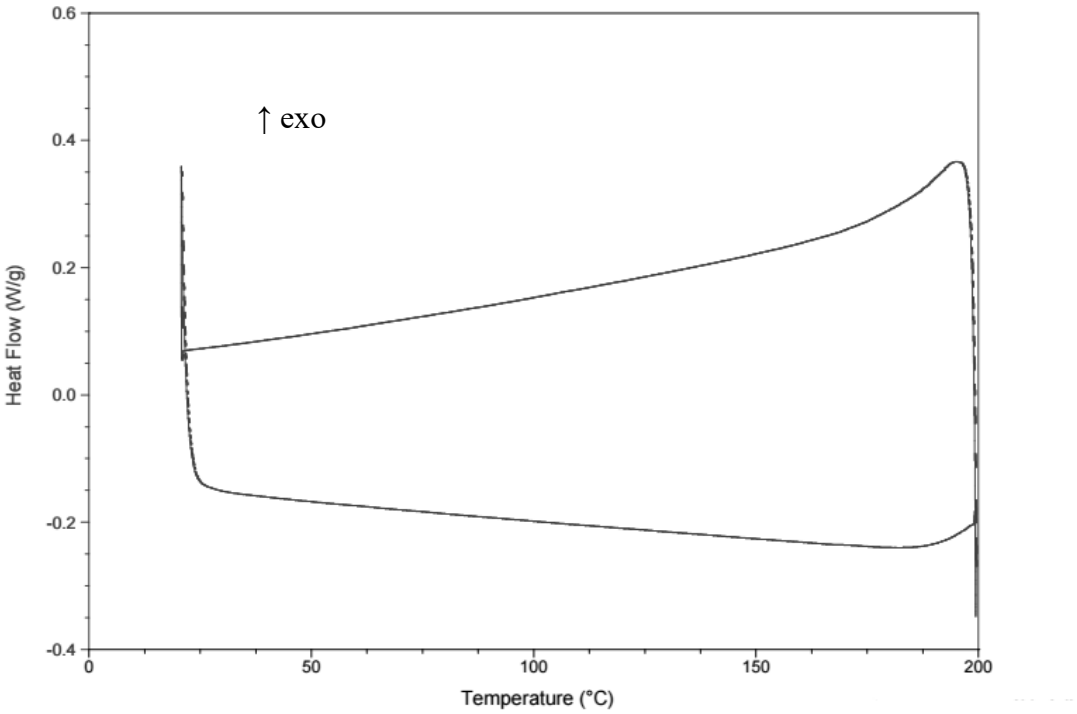

Fig. S20 DSC thermogram collected for **[(BF$_2$L)-(hex$_2$Fl)]$_n$**.

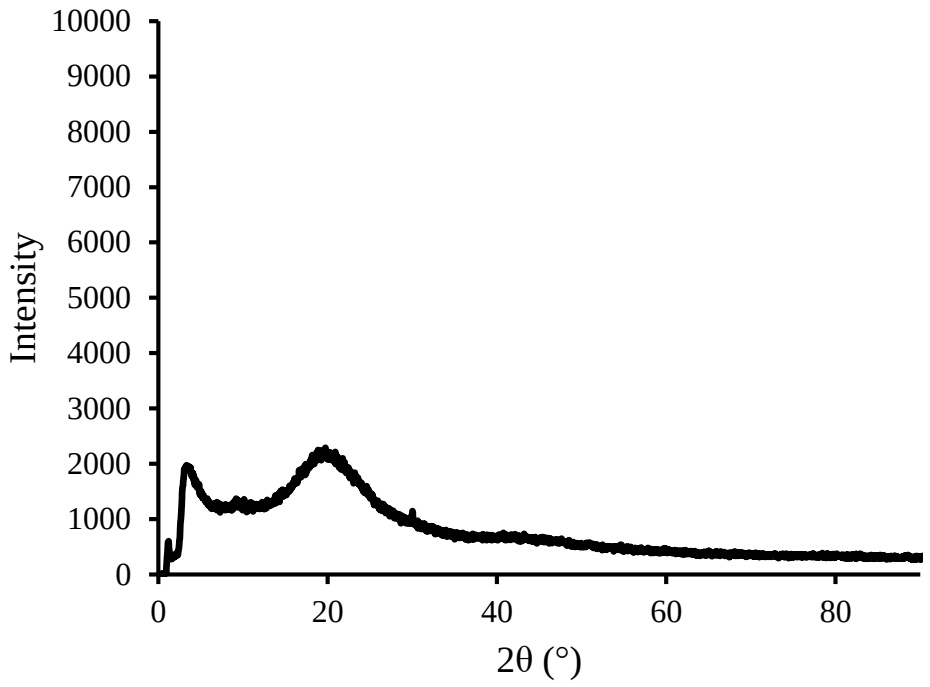

Fig. S21 Powder X-ray diffractogram for **[(BF$_2$L)-(hex$_2$Fl)]$_n$** collected on a glass slide.

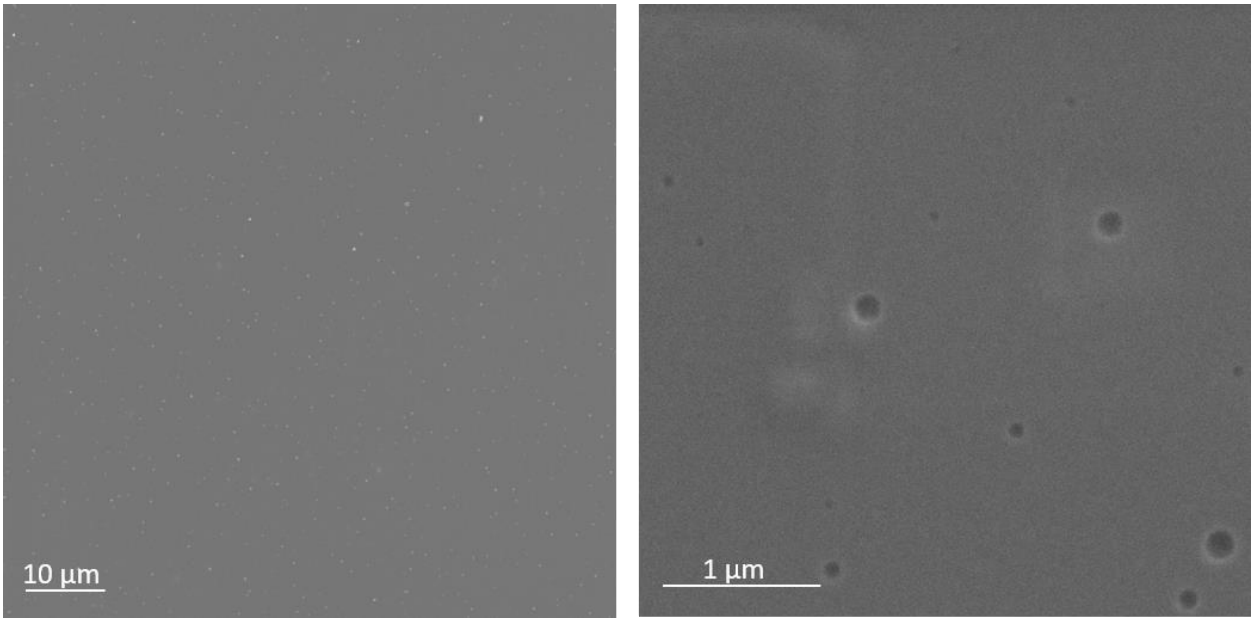

Fig. S22 SEM images of a thin film of **[(BF$_2$L)-(hex$_2$Fl)]$_n$** prepared from a chlorobenzene solution on a silicon wafer.

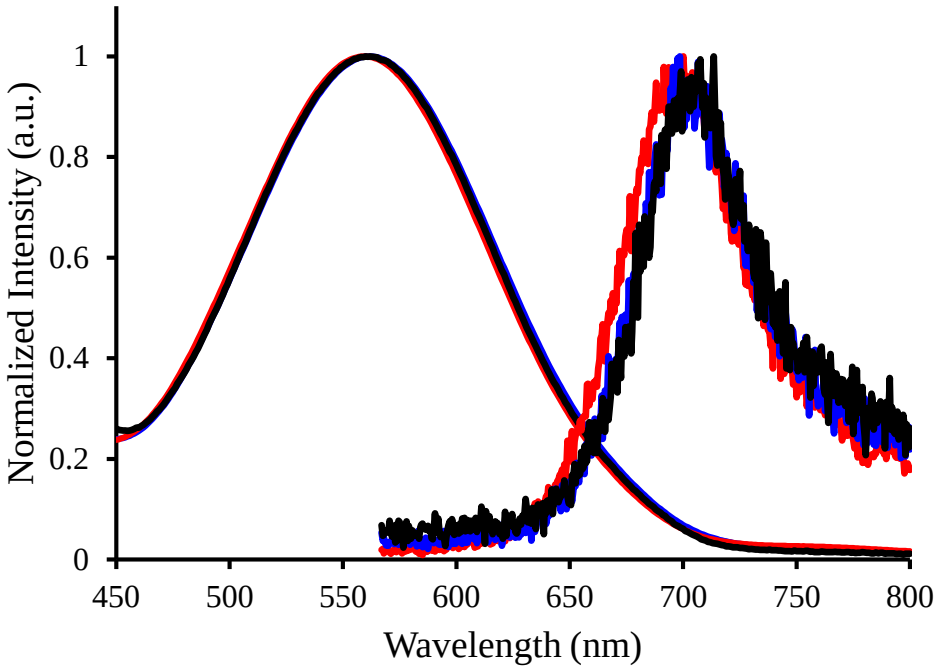

Fig. S23 Normalized UV-vis absorption and emission spectra of **[(BF$_2$L)-(hex$_2$Fl)]$_n$** with number average molecular weight of 6,000 g mol^{-1} (red), 10,000 g mol^{-1} (blue) and 17,000 g mol^{-1} (black) for 10^{-5} M DMF solution.

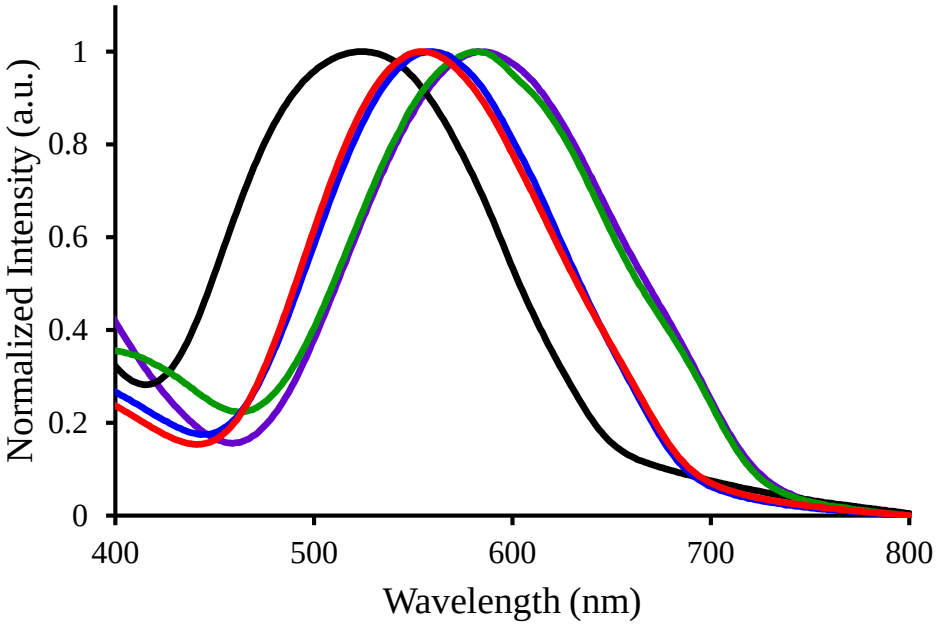

Fig. S24 Normalized thin-film UV-vis absorption spectra of **BF$_2$L** (black), **(BF$_2$L)-(hex$_2$Fl)** (red), **(hex$_2$Fl)-(BF$_2$L)-(hex$_2$Fl)** (green), **(BF$_2$L)-(hex$_2$Fl)-(BF$_2$L)** (blue), and **[(BF$_2$L)-(hex$_2$Fl)]$_n$** (purple).

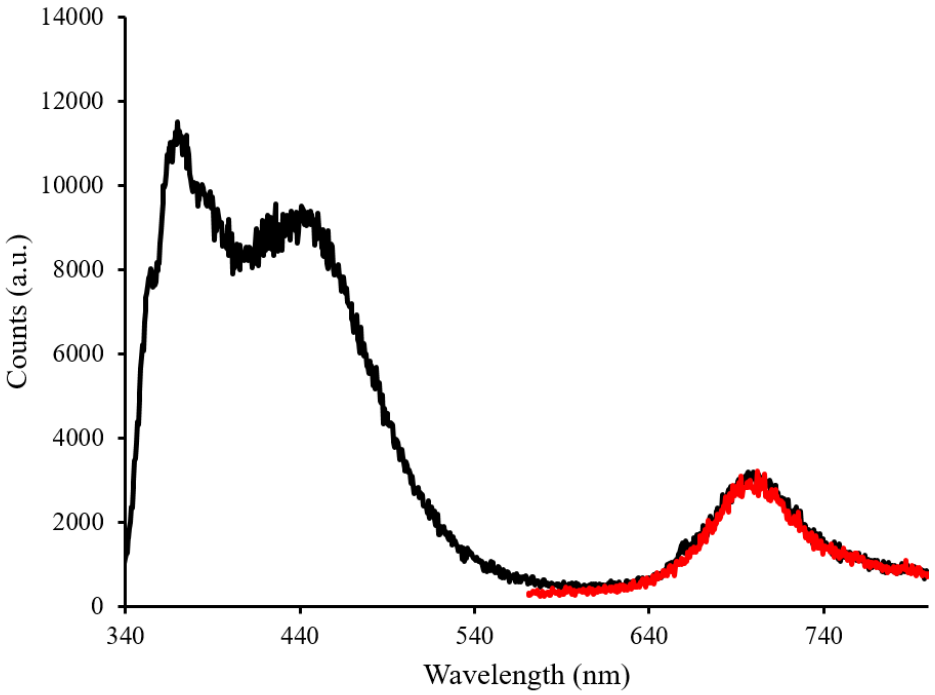

Fig. S25 Emission spectra of **[(BF$_2$L)-(hex$_2$F)]$_n$** recorded at excitation wavelength of 327 nm (black) and 557 nm (red) for a 10^{-5} M degassed DMF solution.

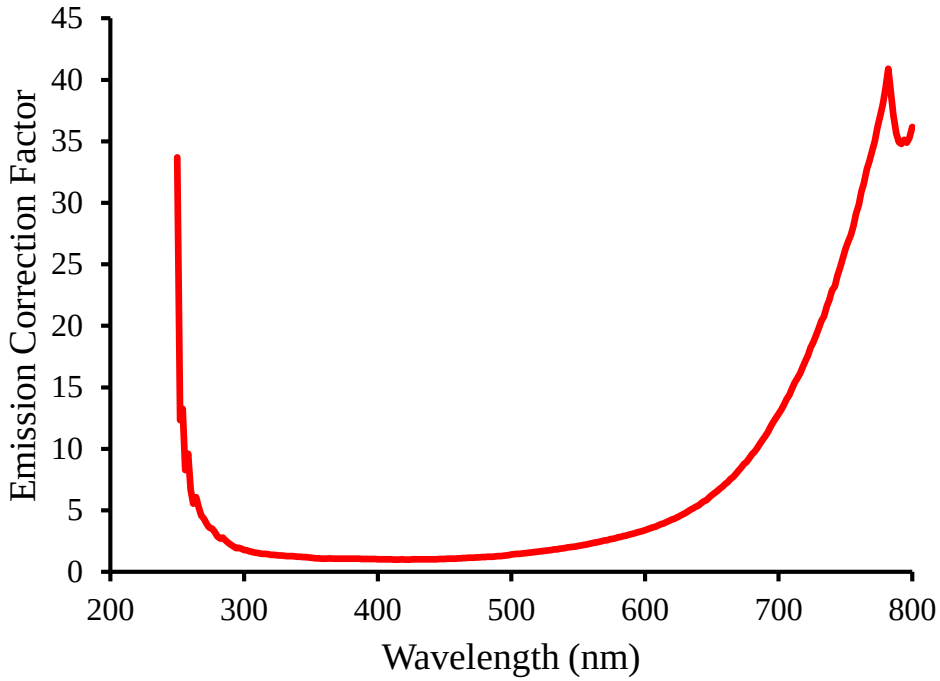

Fig. S26 Wavelength-dependent emission intensity correction provided by Photon Technology International.

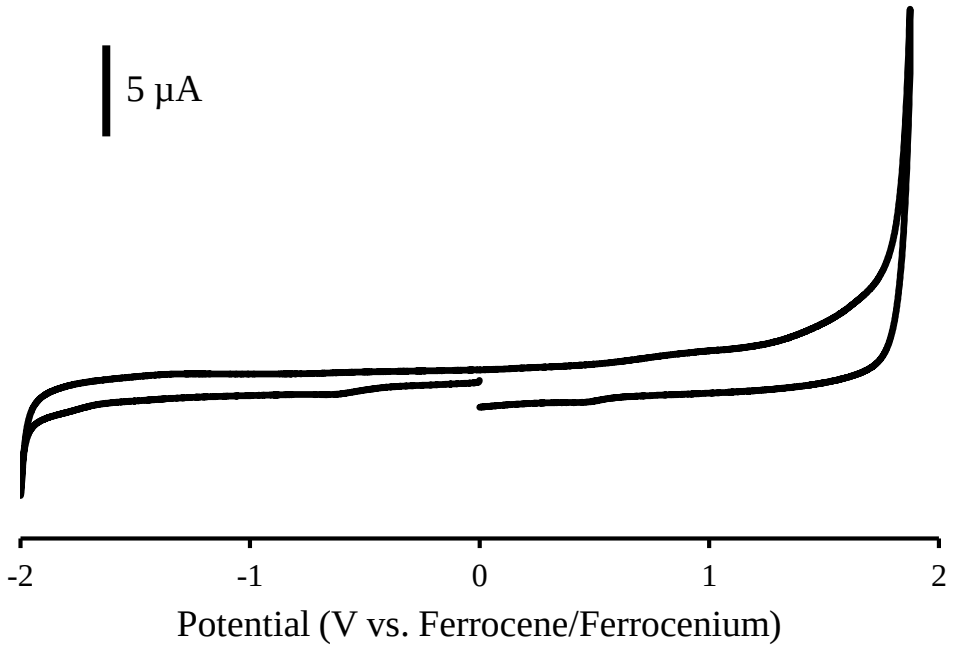

Fig. S27 Cyclic voltammogram of **hex$_2$Fl** recorded at 100 mV s^{-1} in a 1 mM DMF solution containing 0.1 M *n*Bu_4NPF_6 as supporting electrolyte.

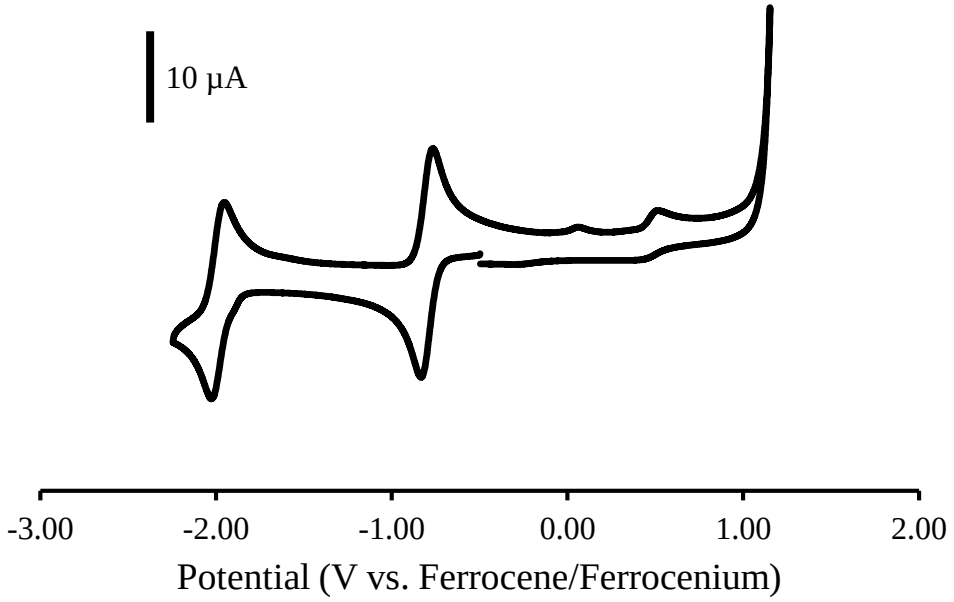

Fig. S28 Cyclic voltammogram of **BF_2L** recorded at 100 mV s^{-1} in a 1 mM DMF solution containing 0.1 M *n*Bu_4NPF_6 as supporting electrolyte.

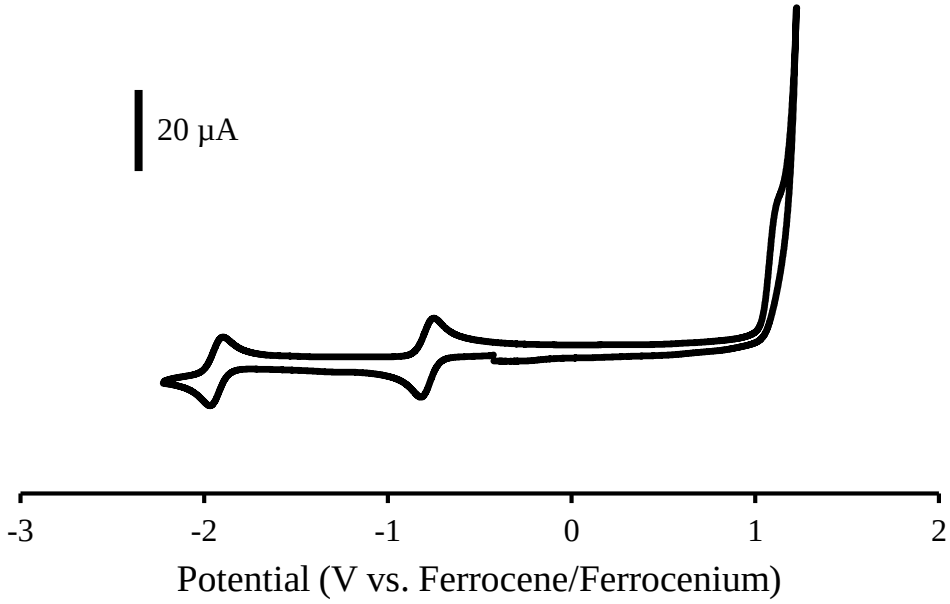

Fig. S29 Cyclic voltammogram of **(BF_2L)-(hex$_2$Fl)** recorded at 100 mV s^{-1} in a 1 mM DMF solution containing 0.1 M *n*Bu_4NPF_6 as supporting electrolyte.

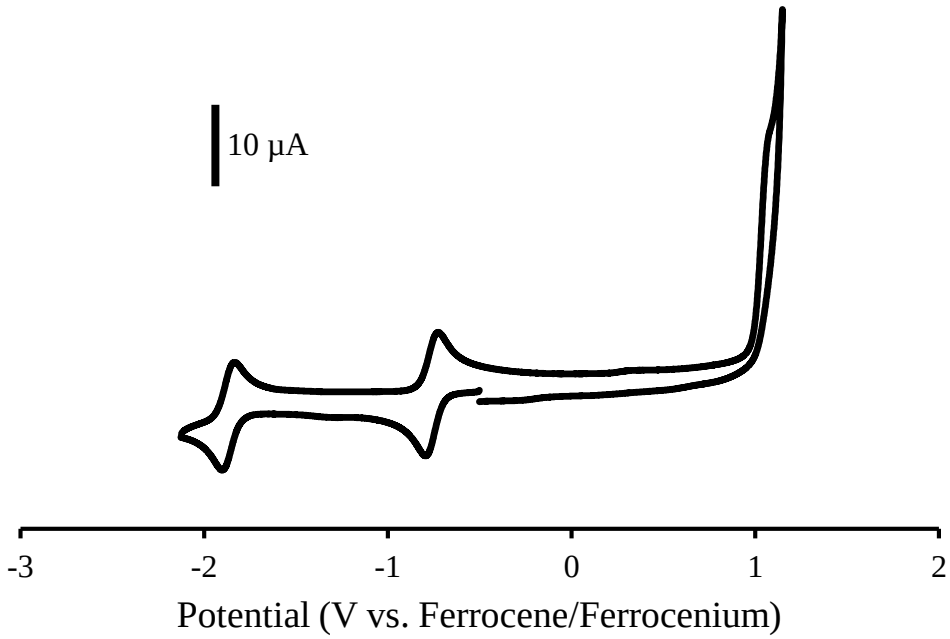

Fig. S30 Cyclic voltammogram of **(hex$_2$Fl)-(BF_2L)-(hex$_2$Fl)** recorded at 100 mV s^{-1} in a 1 mM DMF solution containing 0.1 M *n*Bu_4NPF_6 as supporting electrolyte.

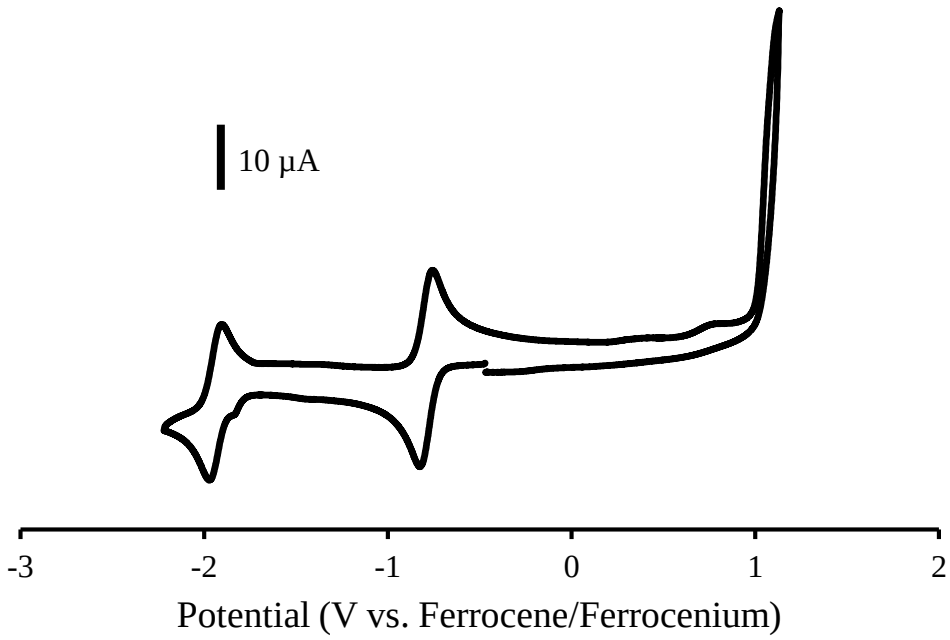

Fig. S31 Cyclic voltammogram of **(BF_2L)-(hex$_2$Fl)-(BF_2L)** recorded at 100 mV s^{-1} in a 1 mM DMF solution containing 0.1 M *n*Bu_4NPF_6 as supporting electrolyte.